# Accepted Manuscript


Isoalantolactone derivative promotes glucose utilization in skeletal muscle cells and increases energy expenditure in db/db mice via activating AMPK-dependent signaling

Deepti Arha, E. Ramakrishna, Anand P. Gupta, Amit K. Rai, Aditya Sharma, Ishbal Ahmad, Mohammed Riyazuddin, Jiaur R. Gayen, Rakesh Maurya, Akhilesh K. Tamrakar

PII: S0303-7207(17)30389-1

DOI: 10.1016/j.mce.2017.07.015

Reference: MCE 10014

To appear in: *Molecular and Cellular Endocrinology*

Received Date: 21 February 2017

Revised Date: 16 June 2017

Accepted Date: 19 July 2017

Please cite this article as: Arha, D., Ramakrishna, E., Gupta, A.P., Rai, A.K., Sharma, A., Ahmad, I., Riyazuddin, M., Gayen, J.R., Maurya, R., Tamrakar, A.K., Isoalantolactone derivative promotes glucose utilization in skeletal muscle cells and increases energy expenditure in db/db mice via activating AMPK-dependent signaling, *Molecular and Cellular Endocrinology* (2017), doi: 10.1016/j.mce.2017.07.015.

# Isoalantolactone derivative promotes glucose utilization in skeletal muscle cells and increases energy expenditure in db/db mice via activating AMPK-dependent signaling

**Deepti Arha[a, d#], E. Ramakrishna[b#], Anand P. Gupta[c], Amit K. Rai[a], Aditya Sharma[a], Ishbal Ahmad[a], Mohammed Riyazuddin[c], Jiaur R. Gayen[c], Rakesh Maurya[b], Akhilesh K. Tamrakar[a, d*]**

[a]*Biochemistry Division, CSIR-Central Drug Research Institute, Lucknow-226031*

[b]*Medicinal and Process Chemistry Division, CSIR-Central Drug Research Institute, Lucknow-226031*

[c]*Pharmacokinetics and Metabolism Division, CSIR-Central Drug Research Institute, Lucknow-226031*

[d]*Academy of Scientific and Innovative Research, New Delhi 110001,India.*

[#]Equal contribution

***Corresponding authors**

**Dr. Akhilesh Kumar Tamrakar**

Division of Biochemistry, CSIR-Central Drug Research Institute

Sec-10, Jankipuram Extension, Sitapur Road, Lucknow-226031, India

E-mail: akhilesh_tamrakar@cdri.res.in

Tel: +91-0522-2772550 Ext. 4635

Fax: +91-0522-2771941

**Abstract**

Augmenting glucose utilization and energy expenditure in skeletal muscle via AMP-activated protein kinase (AMPK) is an imperative mechanism for the management of type 2 diabetes. Chemical derivatives (**2a-2h**, **3, 4a-4d, 5**) of the isoalantolactone (K007), a bioactive molecule from roots of *Inula racemosa* were synthesized to optimize the bioactivity profile to stimulate glucose utilization in skeletal muscle cells. Interestingly, **4a** augmented glucose uptake, driven by enhanced translocation of glucose transporter 4 (GLUT4) to cell periphery in L6 rat skeletal muscle cells. The effect of **4a** was independent to phosphatidylinositide-3-kinase (PI-3-K)/Akt pathway, but mediated through Liver kinase B1 (LKB1)/AMPK-dependent signaling, leading to activation of downstream targets acetyl coenzyme A carboxylase (ACC) and sterol regulatory element binding protein 1c (SREBP-1c). In db/db mice, **4a** administration decreased blood glucose level and improved body mass index, lipid parameters and glucose tolerance associated with elevation of GLUT4 expression in skeletal muscle. Moreover, **4a** increased energy expenditure via activating substrate utilization and upregulated the expression of thermogenic transcription factors and mitochondrial proteins in skeletal muscle, suggesting the regulation of energy balance. These findings suggest the potential implication of isoalantolactone derivatives for the management of diabetes.

***Keywords:*** Insulin resistance, Isoalantolactone, Energy metabolism, Inula racemosa, Glucose utilization.

## 1. Introduction

Type 2 diabetes mellitus (T2DM) is characterized by abnormal insulin secretion and insulin resistance, leading to derangements in carbohydrates, lipid and proteins metabolism (Kahn, 2003). Insulin resistance is a complex pathophysiological condition characterized by impaired insulin action in metabolic tissues, including skeletal muscle, liver and adipose (Kahn et al., 2006). From these tissues, skeletal muscle account for ~40% of the total body mass and is the major site for glucose utilization and homeostasis (Engeli, 2012). A major pathogenic defect in diabetes has been characterized by the impeded capacity of peripheral tissues, most notably the skeletal muscle to utilize glucose effectively in face of hyperinsulinemia (Petersen and Shulman, 2006). This leads to simultaneous rise in blood glucose level and ends up with diabetes.

Obesity is the major risk factor for the development of insulin resistance. Obesity develops when energy intake exceeds energy expenditure. Increased energy retention due to lack of expenditure predisposes an individual towards obesity which cause insulin resistance and further T2DM (Tseng et al., 2010). While current obesity management is focused on reducing caloric intake, increasing energy expenditure has been suggested as an alternative approach for the disease management. This imply specially in case of adaptive thermogenesis in which energy is released in the form of heat and occurs primarily in the mitochondria of skeletal muscle and brown adipocytes (Tseng et al., 2010). Skeletal muscle is an important tissue for exercise-induced thermogenesis (Himms-Hagen, 2004). In skeletal muscle, AMP-activated protein kinase (AMPK) acts as a major modulator of fuel preference and energy metabolism (Hardie et al., 2012). Pharmacological activation of AMPK imparts pseudo effect of exercise and is beneficial for patients with T2DM (Winder and Hardie, 1999). Activation of AMPK results in stimulation of glucose uptake inside the muscle cell driven by enhanced rate of translocation of glucose

transporter 4 (GLUT4) to the cell surface and inhibit glucose output from liver (Hardie et al., 2013; Huang and Czech, 2007). At the same time, chronic activation of AMPK enhances mitochondrial function in skeletal muscle (Koh et al., 2008). Therefore, interventions with ability to activate AMPK in skeletal muscle can modulate glucose utilization and energy metabolism as well for the management of T2DM.

Traditional medicines from plants have an enormous potential to cure various diseases and have been most valuable source of drug leads and to provide useful structural architectures that feature selective and potential access to new biological targets (Newman and Cragg, 2012). Eudesmanolide type sesquiterpene lactones are an excellent example of natural products with wide variety of activities (Di et al., 2014; Chen et al., 1994). They built from three isoprene units and characterized by the presence of exomethylene/methyl at C-4 and C-11 position. They have been reported to show wide range of biological activities, like antiproliferative, anti-inflammatory (Lajter et al., 2014), antiviral, antimicrobial (Ciric et al., 2012), cytotoxic (Rosselli et al., 2012), and lipid lowering activities (Jiang et al., 2011). Isoalantolactone is one among eudesmanolide type sesquiterpene lactones. This compound is widely distributed in *Inula* species, and revealed to possess cytotoxic, anti allergic, anti cancer, anti mycobacterial and antioxidant activities (Xiang et al., 2016; Cantrell et al., 1999; Seo et al., 2009, Li et al., 2016).

As part of our ongoing research program in the area of natural products for the management of diabetes, we explored roots of *Inula racemosa*, an ornamental plant, widely distributed in India, China and Europe. This plant is a rich source of eudesmanolide type sesquiterpene lactones, in particular isoalantolactone and alantolactone (Ma et al., 2013). Ajani *et. al.* (2009) has reported the anti diabetic activity of the methanolic extract of *I. racemosa*, but the precise active ingredient responsible for the antidiabetic activity and the modes of action of

this plant are largely unknown. Here, we investigated the chemical constituents of *I. racemosa* and isolated isoalantolactone (**1**, K007) as a potent stimulator of glucose transport in skeletal muscle cells. Further, we synthesized fourteen derivatives (**2a-2h**, **3, 4a-4d, 5**) of K007 to optimize its bioactivity. Derivatization of isoalantolactone was done by N-substistuted piperizines on C-13 position, allylic hydroxylation followed by esterification at C-3 position. All the derivatives were initially evaluated for effect on glucose uptake in skeletal muscle cells and the active one was subjected to detail mechanistic analysis and *in vivo* efficacy to regulate glucose homeostasis in db/db mice. We report that isoalantolactone derivative **4a** stimulates glucose utilization in clonal skeletal muscle cells and exerts potent antidiabetic effects through modulating energy expenditure in db/db via LKB1/AMPK-dependent signaling.

## 2. Materials and Methods

### 2.1. Materials

Cell culture medium (DMEM), antibiotic/antimycotic solution, fetal bovine serum, and trypsin were from Gibco, USA. 2-deoxyglucose, O-phenylenediamine dihydrochloride, protease inhibitor cocktail, polyclonal anti-*myc*, monoclonal anti-actinin-1, dosromorphin, wortmannin and all other chemicals unless otherwise noted were from Sigma Chemical (St. Louis, MO). 2-Deoxy-D-[$^{3}$H]-glucose (2-DG) was from MP Biomedicals. Antibodies to phospho-Akt (Ser-473), Akt, phospho-AMPKα (Thr-172), AMPKα, phospho-ACC (Ser-79), phospho-LKB1 (Ser-428), LKB-1, p-SREBP-1c (Ser-372), COX IV, Cytochrome C, hexokinase II and GLUT4 (1F8) were from Cell Signaling Technology (USA). Antibody to GLUT1 was from Santa Cruz

Biotechnology, Inc (USA). Triglycerides and total cholesterol measurement kits were from Dialabs and insulin level was measured by mouse insulin ELISA kit (RayBiotech Inc).

### 2.2. Extraction and isolation of isoalantolactone (K007)

The roots of *Inula racemosa* were procured from local market and identified in the Botany Division of CDRI. The voucher specimen (3853) is preserved in the herbarium of the Institute for future reference. The air dried powdered roots were extracted five times with ethanol at room temperature. The combined EtOH extract was filtered and concentrated under vacuum, which afforded a dark brown residue (C002). The crude ethanolic extract was dissolved in distilled $H_2O$ and fractionated with *n*-hexane (F003), chloroform (F004) and *n*-butanol (F005) to afford respective solvent fractions. Based on bioactivity, the *n*-hexane fraction was taken up for a detail chemical investigation. The fraction (F003) was dissolved in chloroform, adsorbed over silica gel (60-120 mesh, 220 g) and subjected to column chromatography (60-120 mesh, 4.0 Kg). The column was eluted with a mixture of hexane: ethyl acetate (96:04) and afforded a white crystalline compound (**1**, K007), which was characterized as isoalantolactone by $^{1}H$, $^{13}C$, IR spectral data.

### 2.3. Cell culture

L6 skeletal muscle cells and L6 cells stably expressing rat GLUT4 with a *myc* epitope inserted in the first exofacial loop (L6-GLUT4*myc*), a kind gift of Dr. Klip, Program in Cell Biology, The Hospital for Sick Children, Toronto, Canada were maintained in DMEM supplemented with 10% FBS and 1% antibiotic/antimycotic solution in a humidified atmosphere of air and 5% $CO_2$ at

$37^0$C. Differentiation was induced by switching confluent cells to medium supplemented with 2% FBS. Experiments were performed in differentiated myotubes 5-6 days after seeding.

**2.4. Glucose uptake measurement**

Glucose uptake inside the myotubes was measured using [$^3$H] 2-deoxy-D-glucose (2-DG), a non metabolizable analog of D-glucose, as the substrate as described previously (Tamrakar et al., 2010). Briefly, myotubes were treated as indicated with final 3h in serum-deprived medium and a sub-set of cells were stimulated with 100 nM insulin for 20 min. Myotubes were then incubated in HEPES-buffered saline supplemented with 10 µM 2-DG (0.5 µCi/ml 2-[$^3$H] DG) for 10 min at room temperature, followed by cell lysis and measurement of radioactivity incorporated by scintillation counting. Nonspecific uptake was determined in the presence of cytochalasin B (50 µM) during the assay. Glucose uptake measured in triplicate and normalized to total protein, was expressed as fold induction with respect to unstimulated cells.

**2.5. GLUT4 translocation measurement**

GLUT4 translocation to cell surface was determined in L6-GLUT4*myc* myotubes by measuring the cell surface level of GLUT4*myc* by an antibody-coupled colorimetric assay as previously described (Tamrakar et al., 2011). The fraction of GLUT4*myc* at the cell surface, measured in triplicate, was expressed as fold induction with respect to unstimulated cells.

**2.6. Assessment of cell viability**

Cell viability was determined by 3-(4, 5-dimethylthiazol-2-yl)-2, 5-diphenyltetrazolium bromide (MTT) assay (Mosmann, 1983). After indicated treatments, the cells were incubated with MTT

solution (5 mg $mL^{-1}$ in PBS) for 4h and the absorbance was measured at 540 nm using an ELISA plate reader (Bioteck, USA).

**2.7. Western analysis**

After indicated treatments, myotubes or tissue samples were lysed in RIPA buffer supplemented with protease and phosphatase inhibitors. Lysates were cleared by centrifugation at 10000 rpm for 10 min at $4^0$C and protein content was measured by the BCA assay. For western blotting, proteins were boiled in Laemmli buffer, separated by SDS-PAGE and transferred onto PVDF membrane. Membranes were then blotted using primary antibodies (4°C overnight), washed and peroxidase-coupled secondary antibody was applied for 1h at room temperature. Membranes were developed using enhanced chemiluminescence (ECL, Millipore), and analyzed using NIH Image J software.

**2.8. Determination of cellular ATP levels**

The cellular ATP levels were estimated in L6 myotubes by Stay Brite ATP assay Kit (Biovision) as per manufacturer's protocol. Briefly, after the indicated incubation, harvested cells were lysed in the reaction buffer and cellular debris was removed by centrifugation. The cellular level of ATP was determined by mixing the supernatant with luciferase reagent that catalysed the light production from ATP and luciferin. Luminescence was measured by a luminometer. Protein concentrations were measured using BCA protein assay kit. The ATP level in each sample was expressed as pmol $\mu g^{-1}$ protein.

**2.9. Animals**

Male C57BL/KsJ-db/db mice (40±5 g) used for the study were kept in polypropylene cage in group of 5-6 animals/cage. The work with these animals was cleared by Institutional Animal Ethics Committee (IAEC) and was conducted in accordance with the guidelines of the Committee for the purpose of Control and Supervision of Experiments on Animals (CPCSEA) formed by the Government of India. Mice were housed under standard conditions of temperature 23 $\pm 2^0$C with relative humidity (50–60%), light 300 Lx at floor level along with light and dark cycles of 12h. Animals were provided with standard diet and drinking water *ad libitum*.

**2.10. Antidiabetic efficacy in db/db mice**

The animals were divided into groups of six animals each. Group I was regarded as the control group and treated with vehicle, whereas the remainder was termed as compound-treated groups and dosed orally at the doses of 3,10 and 30 mg $kg^{-1}$ of compound or metformin (250 mg $kg^{-1}$) for 15 days. Blood glucose level and body weight of each animal was measured at two days interval. On day 15, an oral glucose tolerance test (OGTT) of each animal was performed after an overnight fast. The baseline blood glucose level was monitored at 0 min, followed by an oral glucose load of 3 g $kg^{-1}$ body weight. The blood glucose levels were again checked at 30 min, 60 min, 90 min, and 120 min post-glucose administration, using a glucometer. Blood had withdrawn from the retro-orbital plexus of the eye for the estimation of serum lipid profile and insulin.

**2.11. Comprehensive laboratory animal monitoring system (CLAMS)**

The Comprehensive Laboratory Animal Monitoring System (CLAMS, Columbus Instruments, Columbus, OH) is a set of live-in cages for automated, non-invasive and simultaneous monitoring of horizontal and vertical activity, feeding and drinking, oxygen consumption and

CO2 production. The db/db mice treated with compound, along with control animals were individually kept in CLAMS cages with a 12-h light/12-h dark cycle in an ambient temperature of 22-24°C, and monitored over 3-day period. Mice were kept conscious and unrestrained during the measuring period. Food and water consumption are measured directly as accumulated data. $VO_2$ and $VCO_2$ rates were determined under Oxymax system settings as follows: air flow, 0.8 L $min^{-1}$; sample flow, 0.4 L $min^{-1}$. The expired air was analyzed for a 5 sec period every 7 min using an electrochemical $O_2$ analyzer and a $CO_2$ sensor. The system was calibrated against a standard gas mixture to measure $O_2$ consumed ($VO_2$, ml $kg^{-1}$ $h^{-1}$) and $CO_2$ generated ($VCO_2$, ml $kg^{-1}$ $h^{-1}$). Metabolic rate ($VO_2$) and respiratory exchange ratio (RER) ($VCO_2/VO_2$, ml $kg^{-1}$ $h^{-1}$) were evaluated over a 3-day period. Energy expenditure (kcal $kg^{-1}$ $h^{-1}$; heat production) was calculated using a rearrangement of the Weir equation as supplied by Columbus Instruments: $(3.815+1.232*RER)*VO_2$. A mean of 100 determined values per mice was averaged for the final value of each dark/light cycle. Resting VO2 measured during none to less than baseline activity (0–10 counts/10 min) served as a measure of basal or resting metabolic rate.

**2.12. Tissue triglyceride and total cholesterol measurement**

After the treatment period, mice were sacrificed, and the liver and skeletal muscle tissue sample were excised and frozen in liquid nitrogen for further analysis. Triglyceride levels were measured in 150 mg tissue sample homogenized in 300µl of homogenization buffer (18 mM Tris, pH 7.5, 300 mM mannitol, and 50 mM EGTA). After homogenization, 5ml of chloroform-methanol mixture (2:1) was added and the sample was incubated at room temperature for an hour with occasional vortexing. Post incubation, 1ml of Milli-Q water was added to the sample, mixed thoroughly and centrifuged at 4,700 rpm at 4ºC. The lower organic phase was carefully collected

in a glass tube and solvent was evaporated in nitrogen dryer (Hall et al., 2014). Dried samples were resuspended in 0.5% Triton X-100 by sonication. To estimate triglyceride in the sample, 10µl of this mixture was added to the 1ml of triglyceride reagent (Dialab) and incubated for 10 minute at 37ºC followed by measurement of optical density at 500 nm. Total cholesterol level was measured with Dialab reagent in similar way as triglycerides.

### 2.13. RNA extraction and gene expression analysis

Total RNA was extracted from the tissue by isothiocyabate/phenol/chlorofrom (Trizol) method. Complementary DNA was prepared using Verso cDNA synthesis kit (Thermo Scientific). For semi-quantitative analysis cDNA was amplified by PCR using gene specific primers. 18S rRNA was taken as internal loading control. List of primers is given in table 1.

### 2.14. Statistical analysis

Values are given as mean ± SEM. Analysis of statistical significance of differences in measurements between samples was done by two-way ANOVA or one-way ANOVA with Dunnets post hoc test (GraphPad Prism version 3). $P<0.05$ was considered statistically significant.

## 3. Results

### 3.1. Effect of K007 on glucose uptake in skeletal muscle cells

Glucose uptake inside the skeletal muscle cells is the rate limiting step in its utilization. In an attempt to identify natural molecules that could stimulate glucose uptake like insulin, activity

guided fractionation of the ethanolic extract of the roots of *I. racemosa* led to the identification of an isoalantolactone, K007 (**1**, Fig. 1A) as a potential stimulator of glucose uptake in skeletal muscle cells. Incubation of L6 myotubes with K007 significantly increased basal glucose uptake, with 1.4- and 2.5-fold ($p<0.01$) stimulation at 2.5 and 5.0 μM concentrations, respectively (Fig. 1B). The effect of K007 on insulin-stimulated glucose uptake was determined by incubating the cells with K007, followed by acute insulin treatment (100 nM, 20min). Insulin alone caused 1.46-fold ($p<0.05$) increase in glucose uptake; prior treatment with K007 resulted in an increase of insulin response in an additive manner (Fig. 1B). The effect of K007 on glucose uptake in L6 myotubes was found to be concentration-dependent at 2.5 and 5.0 μM, however further increase in concentration lead to drastic decrease in the rate of glucose uptake (Fig. 1B). Therefore, we evaluated the effect of K007 on viability of L6 myotubes by MTT. Overnight treatment with lower doses of K007 (2.5 and 5.0 μM) had no significant effect on cell viability; further increase in concentration significantly decreased the viability of L6 myotubes in a concentration-dependent manner (Fig. 1C).

### 3.2. Synthesis and the effect of K007 derivatives on glucose uptake in muscle cells

To ward off the deleterious effect of the K007 and optimize its efficacy as a stimulator of peripheral glucose utilization, a series of derivatives (**2a-2h**, **3, 4a-4d, 5**) were synthesized with the structural modification on the basic scaffold. Michael addition is the most frequent reaction to derivatize $\alpha$, $\beta$-unsaturated carbonyl compounds, hence we chose the reaction, to understand the role of exocyclic double bond present at C-11 position, with *N*-substituted piperazines to give Michael addition products (**2a-2h,** Fig. 1, Scheme 1) and other exocyclic double bond at C-4 was reacted with $Sc(OTf)_3$ to form the alloalantolactone (**5,** Fig. 2, Scheme 2) which is an analogue

of isoalantolactone formed by 1,3-H shift. Our further approach for the chemical transformation of K007 was allylic hydroxylation followed by esterification using $SeO_2$, DCC, DMAP and different type carboxylic acids to yield respective esters (**4a-4d,** Fig. 2, Scheme 3). Structural elucidation of the derivatives was performed using $^{1}H$, $^{13}C$, IR spectral data.

In order to determine the potential activity of these derivatives, we analyzed their effects to stimulate glucose uptake in muscle cells. L6 myotubes were incubated with derivatives at 5 µM concentration for overnight period and glucose uptake was measured. Results depicted in the Table 2 illustrate that different derivatives showed diverse efficacy to modulate the rate of glucose uptake in L6 myotubes. The most significant increase in glucose uptake was observed with derivatives **4a**, **4b** and **4c** (3.5-, 2.2- and 2.5-fold, respectively, $P<0.01$). Among them, **4a** was found to be most active, and evaluated for the effect on cell viability. In contrast to the parent compound (K007, **1**), **4a** did not exert any significant effect on cell viability at the concentrations ranged from 2.5 µM to 50 µM, after an overnight incubation, as assessed by the MTT assay (Fig. 3C) and considered safe at these treatment conditions.

### 3.3. Concentration- and time-dependent effect of 4a on glucose uptake

Treatment with **4a** increased glucose uptake in L6 myotubes in a concentration-dependent manner (Fig. 3A) with maximum stimulation of basal glucose uptake at 5.0 µM (3.2-fold, $p<0.001$). Further increase in concentration did not cause any further augmentation in the rate of glucose uptake, indicating the saturation level. Furthermore, **4a** was found to exert a dose-dependent increase of insulin response in an additive manner. Significant response was observed from 5 µM concentration of **4a** (Fig. 3A: control, 1.9-fold vs. **4a**, 4.6-fold, $p<0.001$).

Incubation of L6 myotubes with **4a** (5 µM) resulted an increase in the rate of glucose uptake in a time-dependent fashion under both basal and insulin-stimulated conditions (Fig. 3B) with significant stimulation of basal glucose uptake after 6h. Maximum stimulation by **4a** was observed after 16 h, and in all subsequent experiments 16 h incubation was used.

### 3.4. Effect of 4a on GLUT4 translocation to the cell surface in muscle cells

Enhanced translocation of GLUT4 to cell periphery is an essential mechanism for inducible glucose uptake inside the cells. To investigate the glucose uptake stimulatory effect, **4a** was probed for its ability to enhance GLUT4 translocation in L6-GLUT4*myc* myotubes. Consistent with glucose uptake data, overnight incubation with **4a** significantly enhanced the surface GLUT4*myc* level in a concentration-dependent fashion (1.3- and 1.9-fold increase at 2.5 and 5 µM, respectively). Insulin alone resulted in a profound increase in surface GLUT4*myc* level (1.75-fold vs. basal, $p<0.001$). Treatment of myotubes with **4a** for 16 h with insulin added for final 20 min, resulted in dose-dependent increase of insulin response in an additive manner ($p<0.001$, Fig. 3D ).

We next investigated whether the **4a**-mediated raise in surface level of GLUT4*myc* was accompanied by an increase in total amount of GLUT4. Cellular amount of GLUT4 was assessed after overnight incubation. **4a** did not affect the cellular amount of GLUT4 either under basal or insulin-stimulated condition in L6 myotubes. Additionally, treatment with **4a** had no effect on the cellular amount of GLUT1, another major glucose transporter responsible for basal glucose uptake in skeletal muscle cells (Fig. 3E and 3F).

### 3.5. Effect of 4a on PI-3-Kinase-dependent signaling pathway

To investigate the involvement of pathways that contributed to GLUT4 translocation in skeletal muscle, we mapped the effect of **4a** on phosphatidylinositide-3-kinase (PI-3-K) activation, the basic pathway responsible for the metabolic effects of insulin. The effect of wortmannin, a selective inhibitor of PI-3-Kinase pathway (Malide et al., 1997) on **4a**-stimulated glucose uptake was examined in L6 myotubes. As represented in the Fig. 4A, insulin-stimulated glucose uptake was completely abolished by wortmannin ($p<0.01$), but there was no significant effect on **4a**-stimulated glucose uptake in presence of wortmannin. These results suggest that the signal transduction leading to glucose uptake by **4a** is primarily mediated via a PI-3-K-independent pathway. To further validate the finding, we evaluated the phosphorylation of Akt, a downstream key note of PI-3-K pathway, at the regulatory sites Ser-473 and Thr-308. As expected, insulin (100 nM) induced strong phosphorylation of Akt, but **4a** did not cause any significant effect on Akt phosphorylation, and consistent to glucose uptake data, presence of wortmannin profoundly inhibited insulin-stimulated phosphorylation of Akt at Ser-473 and Thr-308 in L6 myotubes (Fig. 4B-D), verifying the action of wortmannin to inhibit PI-3-K mediated signaling.

### 3.6. Effect of 4a on AMPK-dependent pathway

Given the glucose uptake stimulation by **4a** was independent of PI-3-K/Akt pathway; we studied its effect on the AMPK, a sensor of cellular energy status and established to stimulate glucose uptake independent to insulin (Gowans et al., 2013). L6 myotubes were incubated with **4a** (5μM) or established AMPK activator metformin (500μM) in presence of dorsomorphin, a selective inhibitor of AMPK. Dorsomorphin (20 μM) was added 30 min prior to treatment with **4a** or metformin. As shown in Fig. 5A, presence of dorsomorphin inhibited both **4a**- and metformin-stimulated glucose uptake to a significant level ($p<0.01$). These data suggest that **4a**, like

metformin, utilizes an AMPK-dependent pathway to mediate glucose uptake. To confirm the activation of AMPK, we examined the effect of **4a** on phosphorylation of AMPKα at Thr-172, the principle regulatory site of AMPK activation (Hawley et al., 1996). **4a** substantially increased the phosphorylation of AMPKα (Thr-172), in a concentration-dependent manner, without having any significant effect on total cellular content of AMPKα (Fig. 5B)

The major upstream kinase responsible for phosphorylation of AMPKα at Thr-172 is liver kinase B1 (LKB1). To map whether **4a**-mediated activation of AMPKα was LKB1-dependent, we analyzed the effect of **4a** on phosphorylation of LKB1 (Ser-428). Treatment with **4a** augmented the phosphorylation of LKB1 (Ser-428) in a concentration-dependent manner (Fig. 5C). These findings suggest that **4a** utilizes LKB1/AMPK-dependent signaling to stimulate glucose uptake in skeletal muscle cells. AMPK has been established as cellular fuel gauge, activating its kinase activity with decrease in cellular energy charge (Winder and Hardie, 1999). Treatment with **4a** significantly decreased the cellular ATP level in L6 myotubes (Fig. 5D), pointing the activation of cellular processes require energy expenditure.

### 3.7. Effect of 4a on signalling downstream to AMPK

Besides enhancing glucose uptake inside the cells, AMPK also modulate fatty acid metabolism by directly phosphorylating and inactivating its major downstream target acetyl CoA carboxylase (ACC) at Ser-79 (Munday et al., 1998; Davies, 1990). Hence, to study the effect of **4a** on downstream signalling to AMPK, we assessed the phosphorylation of ACC (Ser-79). As expected, **4a** enhanced the phosphorylation of ACC, compared to control (Fig. 5E, $p<0.05$), validating the activation of AMPK by **4a**. Another downstream target of interest was sterol response element binding protein-1c (SREBP-1c), an important lipogenic transcription factor

regulated by exercise, nutritional modification and insulin (Horton et al., 2002). AMPK has been known to phosphorylate SREBP-1c at Ser-372, thereby preventing its proteolytic cleavage and translocation to nucleus and thus attenuating transcription of lipogenic genes (Li et al., 2011). In L6 myotubes, **4a** treatment elevated SREBP-1c (Ser-372) phosphorylation to a significant level (Fig. 5F, $P<0.05$), suggesting that treatments with **4a** may decrease the cellular lipid content.

### 3.8. Metabolic effects of 4a in *db/db* mice

The metabolic effects of **4a** were further evaluated in diabetic db/db mice by administering the compound for 15 days at different doses. There was no significant effect on body weight, but the mean blood glucose of the treated animals decreased gradually, during the course of treatment (Fig. 6 A & B). After the treatment period, animals were subjected to whole body composition analysis by Echo-MRI. Treatment with **4a** significantly reduced the body fat mass at the dose of 30 mg/kg ($p<0.05$), associated with an increase in the lean mass ($p<0.05$). Metformin treatment had no significant effect on body mass composition of db/db mice (Fig. 6G). The mice treated with **4a** showed better tolerance to glucose load in a dose-dependent fashion (Fig. 6C). At the dose of 30 mg/kg, **4a** administration caused 35.2% ($p<0.05$) improvement in glucose tolerance, which is quite comparable to physiological dose of metformin (250 mg/kg), causing 42.4% improvement ($p<0.01$) (Fig. 6D). Skeletal muscle is the major depot for post parandial glucose disposal thereby regulating glucose homeostasis. Treatment with **4a** enhanced the gene expression of GLUT4 and hexokinase, associated with increased GLUT4 protein level, but unaltered hexokinase protein level in skeletal muscle of db/db mice (Fig. 6 E, F, H & I). However, **4a** did not have any significant effect on serum insulin level, whereas metformin caused significant reduction in serum insulin level of db/db mice (Fig. 6J).

To verify the participation of AMPK in **4a**-mediated improvement in glucose metabolism, we checked the activation of AMPK in skeletal muscle of db/db mice. AMPK signaling was up regulated as confirmed by the increased phosphorylation of AMPK (Thr-172), ACC (Ser-79) and LKB1 (Ser-428) in skeletal muscle of **4a** treated mice, compared to control (Fig. 7 A-D). Metformin also significantly up regulated the phosphorylation the AMPK and associated enzymes. Metformin has been reported to increase the phosphorylation of AMPK in liver (Shaw et al., 2005). To verify the effect of **4a** on liver AMPK signaling, we assessed the phosphorylation in liver of db/db mice. Similar to metformin, treatment with **4a** significantly enhanced the phosphorylation of AMPK (Thr-172) and ACC (Ser-79) in liver of db/db mice (Fig. 7 E-G), suggesting the activation of AMPK signaling in liver.

In addition to the beneficial effect on glucose metabolism, activation of AMPK has been shown to exert favorable effect on lipid metabolism through phosphorylation and inhibition of enzymes involved in cholesterol and lipid synthesis (Muoio et al., 1999). Therefore, we investigated the effect of **4a** treatment on serum and tissue levels of cholesterol and triglycerides in db/db mice. Similar to the metformin, treatment with **4a** resulted in a significant decrease in serum and hepatic level of total cholesterol in a dose-dependent fashion (Fig. 7 H & I). Serum triglyceride level was also decreased by lower dose of **4a** (10 mg/kg) or metformin, but there was significant elevation in serum triglyceride level upon treatment with 30 mg/kg dose of **4a** in db/db mice (Fig. 7J). In contrast, the hepatic and skeletal muscle triglyceride levels were significantly decreased by **4a** in db/db mice (Fig. 7 K & L). We further assessed the effect of **4a** on liver lipid metabolism by measuring the expression of key target genes of lipid metabolism in liver of db/db mice. Treatment with **4a** did not cause any significant change in gene expression of ACC, but there was a significant decrease in Stearoyl-CoA desaturase (SCD1). Metformin

treatment did not cause any significant effect on SCD1 expression. Moreover, both **4a** and metformin reduced the expression of SREBP-1c and PPAR-α (Figure 8).

### 3.9. Effect of 4a on energy homeostasis in *db/db* mice

Energy homeostasis is maintained by regulating a delicate balance between energy intake and energy expenditure. Increase in energy intake will lead to obesity as in the case of type 2 diabetes, so is the lack of expenditure. We analyzed the effect of **4a** (30 mg/kg) on energy expenditure using comprehensive lab animal monitoring system (CLAMS). The db/db mice treated with **4a** showed increased oxygen consumption and carbon dioxide production rate than the control animals through a 12h light/dark cycle (Fig. 9 A-D), suggesting the improvement in metabolic profile of the treated animals. Although, there was no significant change in respiratory exchange ratio (RER), implement that the mice were still using the carbohydrate as source of energy (Fig. 9 E & F). The db/db mice treated with **4a** showed significant increase in whole body energy expenditure (in form of heat) with respect to control animals (Fig. 9 G & H). This increase in energy expenditure was not due to the increase in physical activity as revealed by the unaffected x axis and z axis movement (Fig. 10 A & B). There was a significant improvement in basal metabolic rate and resting metabolic rate of **4a**-treated db/db mice, clearly indicating an increase in energy expenditure (Fig. 10 C & D). On the other hand, treatment of **4a** in db/db mice showed an increase in food intake in comparison to control animals (Fig. 10E). But there was no significant difference in body weight of treated animals compared to control mice.

The **4a** treatment induced the activation of a network of genes regulating energy homeostasis and mitochondrial functions in skeletal muscle of db/db mice. The expression of the transcription factors, including PPARα, PGC-1α, NRF1, and Dio2, was increased in skeletal

muscle of the **4a** treated animals (Fig. 11 A & B). The expression of UCP1 and other mitochondrial marker genes such as ATP synthase, COX IV, and Cytochrome C, was also significantly induced (Fig. 11 C & D). Western blot analysis indicated the enhanced protein level of COX IV and Cytochrome C by **4a** treatment in skeletal muscle tissue of db/db mice (Fig. 11 E-G). These lines of evidence suggest that **4a** could enhance energy expenditure by regulating mitochondrial functions in skeletal muscle of db/db mice.

## 4. Discussion

Skeletal muscle is the prominent situate for maintenance of postprandial glucose homeostasis and is the primary tissue contributing to whole-body energy expenditure. In skeletal muscle glucose metabolism is mainly regulated by insulin, which exerts its metabolic actions by activating signaling cascade involving insulin receptor substrate (IRS), PI3K, and Akt, leading to the translocation of GLUT4 from intracellular pool to cell membrane, where they facilitate glucose transport inside the cells (Pessin et al., 1999). Skeletal muscle insulin resistance, the impaired response of insulin to regulate glucose metabolism, is a major factor in the pathogenesis of T2DM (Yu et al., 2002). However, various other stimuli such as osmotic shock (Chen et al., 1997), activation of G-protein coupled receptors (Wang et al., 2000), contraction in skeletal muscle (Yeh et al., 1995) have been reported to induce insulin-like effect to stimulate glucose utilization through insulin-independent pathways. Therefore, targeting insulin independent mechanisms to regulate glucose metabolism may be helpful in management of T2DM.

Obesity represents a major risk factor for the development of insulin resistance and other features of the metabolic syndrome. Obesity develops when there is an imbalance between the

energy intake and energy expenditure, and targeting energy expenditure has proven to be an attractive concept for managing obesity and associated metabolic complications (Tseng et al., 2010). Adaptive thermogenesis, a physiological process whereby energy is dissipated in the form of heat in response to external stimuli provides a mean to target energy expenditure. Skeletal muscle is an important tissue for thermogenesis (Himms-Hagen, 2004). In skeletal muscle AMPK is the central enzyme to regulate cellular bioenergetics, which senses the nutrient status and help to regulate glucose transport, fatty acid oxidation, and metabolic adaptations in skeletal muscle (Koh et al., 2008). Therefore, AMPK activation in skeletal muscle can regulate both the glucose metabolism and cellular bioenergetics, benefecial for the management of metbolic complications, including T2DM.

In an attempt to discover small molecule from natural sources that could stimulate glucose uptake, isoalantolactone (K007) from the roots of *I. racemosa* was identified with potential to augment glucose uptake in L6 myotubes. However, noticing the adverse effect of K007 on cell viability at higher concentration, chemical derivatives of K007 were synthesized to optimize its bio-efficacy without cytotoxic effect. Among the derivatives, **4a** displayed potent stimulation of glucose uptake in L6 myotubes in a concentration- and time-dependent fashion, without affecting the cell viability. The effect of **4a** (5.0 μM) was significantly higher than that of insulin (100 nM) at concentration that produced maximum response. Similar to insulin, **4a** treatment enhanced the rate of GLUT4 translocation to cell surface in skeletal muscle cells, required for the entry of glucose inside the cells (Huang and Czech, 2007). It also potentiated insulin-stimulated glucose uptake and GLUT4 translocation in an additive manner, suggesting that **4a**-induced signaling leading to glucose uptake is distinct from that induced by insulin.

The metabolic actions of insulin are mediated through activation of PI-3-K (Taniguchi et al., 2006). Presence of wortmannin, a specific inhibitor of PI-3-K abolished the insulin mediated stimulation of glucose uptake to basal level. However, in case of **4a**, wortmannin had no effect on glucose uptake stimulation, negating the participation of PI-3-K. Downstream to PI-3-K, Akt has been shown to be involved in insulin stimulated glucose uptake in skeletal muscle cells (Taniguchi et al., 2006). Insulin induced a strong phosphorylation of Akt at Ser-473 and Thr-308, but **4a** did not induce any marked enhancement of Akt phosphorylation. These findings confirm that **4a** stimulated glucose uptake is primarily mediated via a PI-3-K/Akt-independent signaling pathway. The possible candidate for such PI-3-K independent stimulation of glucose uptake might be the AMPK, which is an intracellular fuel sensor and has been shown to play a role in the physiological control of insulin-independent glucose uptake (Rutter et al., 2003). AMPK activation has been established to increase glucose uptake during exercise via stimulating GLUT4 translocation in skeletal muscle cells. Several plant derived bioactive molecules, including metformin have been reported to enhance glucose utilization through AMPK-dependent signaling pathway (Lee et al., 2006; Shaw et al., 2005, Shen et al., 2014). Presence of dorsomorphin, a specific inhibitor of AMPK, inhibited both **4a** and metformin-induced glucose uptake in L6 myotubes, suggesting the participation of AMPK-dependent signaling pathway. AMPK is activated by phosphorylation of Thr-172 residue of its catalytic α subunit (Hawley et al., 2003) by upstream kinase LKB1. The LKB1 kinase is a tumor suppressor protein ubiquitously expressed in mammalian cells and has been shown to phosphorylate and activate AMPK in response to metformin and energy depleted condition (Shaw et al., 2004, Shaw et al., 2005). We also confirmed an increase in the phosphorylation of AMPK (Thr-172) by **4a** in a concentration-dependent manner, indicating the activation of AMPK. It has been reported that

phosphorylation of LKB1 at Ser-428 lead to nuclear export of LKB1 from cytosol, which in turn lead to the phosphorylation of AMPK$\alpha$ (Xie et al., 2008). The **4a** augmented the phosphorylation of LKB1 (Ser-428), pointing the activation of LKB1/AMPK axis. Besides phosphorylation, AMPK is also activated by metabolic stress associated with decreased cellular ATP level. Under such condition AMP and ADP levels increases, leading to allosteric activation of AMPK (Oakhill et al., 2011). Here, treatment with **4a** significantly reduced the cellular ATP level in L6 myotubes, indicating the change in cellular bioenergetics, favoring the activation of AMPK. Data indicate that both activation of LKB1 and decrease in cellular ATP level might participate independently of interdependently to activate AMPK in response to **4a**. These results strongly suggest that activation of AMPK signaling by **4a** in skeletal muscle cells up regulate glucose uptake, independent to insulin signaling.

Activation of AMPK has correlated with its kinase activity resulting in phosphorylation and inhibition of ACC, the rate limiting enzyme controlling fatty acid synthesis. Phosphorylation of ACC accounts for both allosteric and covalent modification components of AMPK activation (Gowans et al., 2013). Consistent to the effect on AMPK, **4a** significantly enhanced the phosphorylation of ACC (Ser-79). Another important target of AMPK related to lipid metabolism is the SREBP. SREBP-1c is a nutritionally regulated lipogenic transcription factor involved in activation of genes of fatty acid and triglyceride synthesis (Horton et al., 2002). AMPK directly interact and stimulate the phosphorylation of SREBP-1c (Ser-372), resulting in the suppression of its cleavage and nuclear translocation to regulate gene expression (Li et al., 2011). Treatment with **4a** resulted in increased phosphorylation of SREBP-1c (Ser-372) in L6 myotubes. It is conceivable from this data that this pathway would play an important role in

regulating lipogenesis in other tissues such as adipose and liver, contributing to improved systemic response.

Inspired from the *in vitro* effects of **4a** on glucose metabolism in L6 myotubes, we examined the effect of **4a** on glucose homeostasis in db/db mice, a well-established model for type 2 diabetes. The administration of **4a** for 15 days led to increased phosphorylation of AMPK (Thr-172), ACC (Ser-79) and LKB1 (Ser-428) in skeletal muscle of db/db mice, validating the *in vitro* effect of **4a** on AMPK signaling. Additionally, there was an increase in the phosphorylation of AMPK (Thr-172) and ACC (Ser-79) in liver of db/db mice treated with **4a** or metformin, suggesting the activation of AMPK signaling in liver. Furthermore, treatment with **4a** resulted in dose-dependent decrease in blood glucose level, without having any significant effect on body weight. The **4a** treated animals displayed a better tolerance to glucose load, which was particularly prominent and comparable to metformin, at the dose of 30 mg/kg. It is worthy of noticing that **4a** stimulates GLUT4 translocation in skeletal muscle cells leading to enhanced glucose uptake, which might be responsible for the improved glucose tolerance in animal system. Moreover, chronic treatment with **4a** was associated with increased expression of the GLUT4 in skeletal muscle of the db/db mice, contributing to improved glucose tolerance. In support to our data, chronic activation of AMPK by AICAR has also been shown to increase skeletal muscle GLUT4 expression in normal rats (Holmes et al., 1999), postulating the ability of chronic AMPK activation to upregulate the proteins that mediate glucose uptake in skeletal muscle, to modulate whole body glucose metabolism.

In addition to the potential therapeutic effects on glucose metabolism, AMPK activation may also have favorable effects on lipid metabolism. Skeletal muscle insulin resistance under obesity is associated with elevated intramuscular lipid levels, raising the possibility that

alterations in lipid metabolism influence insulin signaling (Bonen et al., 2004; Steinberg, 2007). AMPK activation has been shown to inhibit the key enzymes of lipid and cholesterol biosynthesis, suggesting the effect of this kinase to ameliorate dyslipidemia (Muoio et al., 1999). In db/db mice, similar to metformin, treatment with **4a** resulted in a dose-dependent decrease in total cholesterol level in serum and liver. In contrast, serum triglyceride level was significantly elevated by **4a** treatment in db/db mice at higher dose (30 mg/kg). This data conflict the postulated role of AMPK to decrease lipid synthesis, but chronic AICAR treatment has previously been reported to increase serum triglycerides in db/db and ob/ob mice (Halseth et al., 2002). In contrast to the notable increase in serum triglyceride level after **4a** treatment, hepatic and skeletal muscle triglyceride levels were significantly decreased by **4a** in db/db mice. This suggests that increased serum triglycerides level observed upon **4a** treatment was not due to increased production in liver or skeletal muscle. However, the decreased rate of clearance might be possible reason for the elevated serum triglyceride level upon **4a** treatment in db/db mice. Moreover, treatment with **4a** did not cause any significant change in gene expression of ACC, but there was a significant decrease in Stearoyl-CoA desaturase (SCD1), indicating its beneficial effect on liver lipid metabolism. SCD1 catalyzes the rate-limiting step in the biosynthesis of monounsaturated fatty acids and decreased activity of SCD1 facilitates increased energy expenditure and β-oxidation through activating AMPK (Dobrzyn et al., 2004). Moreover, both **4a** treatment reduced the expression of SREBP-1c and PPAR-α, pointing the increase in energy expenditure and decrease in lipid synthesis in liver.

AMPK is a principal regulator of energy metabolism and mitochondrial biogenesis (Zong et al., 2002; Canto et al., 2009). Here, we assessed the effect of **4a**-mediated AMPK activation on body composition and energy balance in db/db mice and found a significant increase in lean

mass and decrease in fat mass, associated with increase in energy expenditure (in form of heat) by **4a** treatment in db/db mice. The food intake was also higher in **4a** treated mice, compared to control. The fact that energy expenditure was enhanced by **4a** treatment throughout the light and dark cycle, but there was no significant difference in physical activity in control or **4a**-treated mice, suggest that substrate oxidation is continuously higher in **4a**-treated mice. In agreement, **4a**-treated mice displayed an increased rate of oxygen consumption and carbon dioxide production, and higher metabolic rates compared to control animals. But there was no significant difference in RER, reflecting the use of carbohydrates over lipid as a source of energy. Taken together, these data suggest that treatment with **4a** accelerates the substrate metabolism in mice and hence displays better glucose tolerance, and inhibits further weight gain.

AMPK has been proposed as a key molecule in eliciting metabolic adaptations to exercise. Pharmacological and exercise-induced activation of AMPK has been reported to increase the expression and activity of several mitochondrial genes and oxidative proteins, including citrate synthase, ATP synthase, cytochrome c oxidase and uncoupling protein 1, and transcription factors, including PPARα, PGC-1α, NRF1, and Dio2 (Suwa et al., 2003; Terada et al., 2002). The **4a** treatment in db/db mice up regulated the expression of thermogenic markers, UCP1, PGC-1α, Dio2 and NRF-1 in skeletal muscle of db/db mice, indicating its effect on energy expenditure through thermogenesis. PGC-1α also acts as a downstream target of AMPK to modulate energy metabolism (Jager et al., 2007). We observed activation of mitochondrial genes including ATP synthase, COX IV, and cytochrome C in skeletal muscle of **4a**-treated db/db mice, suggesting its beneficial effect on mitochondrial functions. Collectively, our data suggested that **4a** could activate AMPK that activate PGC-1α leading to the induction mitochondrial proteins to regulate energy expenditure. In conclusion, our findings establish an

important role for an isoalantolactone derivative (**4a)** in regulating skeletal muscle glucose metabolism and bioenergetics, and provide a basis for further structural activity relationship (SAR) analysis to develop optimized lead from isoalantolactone for the management of T2DM.

**Acknowledgements**

The authors gratefully acknowledge the financial support from Indian Council of Medical Research (ICMR), New Delhi India in the form of ad-hock project (IRIS ID No. 2011-09510). DA and AKR are also thankful to ICMR for financial support in the form of Senior Research Fellowship. We would like to thank Dr Amira Klip for providing L6-GLUT4*myc* cells. This manuscript bears the CDRI communication No. XXXX.

**References**

1. Ajani, H., Patel, H., Shah, G., Acharya, S., Shah, S., 2009. Evaluation of antidiabetic effect of methanolic extract of *Inula racemosa* roots in rats. Pharmacology online 3, 118-129.
2. Bonen, A., Parolin, M.L., Steinberg, G.R., Calles-Escandon, J., Tandon, N.N., Glatz, J.F., Luiken, J.J., Heigenhauser, G.J., Dyck, D.J., 2004. Triacylglycerol accumulation in human obesity and type 2 diabetes is associated with increased rates of skeletal muscle fatty acid transport and increased sarcolemmal FAT/CD36. FASEB J.18, 1144-1146.
3. Canto, C., Gerhart-Hines, Z., Feige, J.N., Lagouge, M., Noriega, L., Milne, J.C., Elliott, P.J., Puigserver, P., Auwerx, J., 2009. AMPK regulates energy expenditure by modulating NAD+ metabolism and SIRT1 activity. Nature 458, 1056-1060.

4. Cantrell, C.L., Abate L., Fronczek, F.R., Franzblau, S.G., Quijano, L., Fischer, N.H., 1999. Antimycobacterial eudesmanolides from *Inula helenium* and *Rudbeckia subtomentosa*. Planta Med. 65, 351-355.

5. Chen, C.H., Yang, L.M., Lee, T.T.Y., Shen, Y.C., Zhang, D.C., Pan, D.J., McPhail, A.T., McPhail, D.R., Liu, S.Y., et al., 1994. Antitumor agents. CLI. Bis(helenalinyl)glutarate and bis(isoalantodiol-B)glutarate, potent inhibitors of human DNA topoisomerase II. Bioorg. Med. Chem. 2, 137-145.

6. Chen, D., Elmendorf, J.S., Olson, A.L., Li, X., Earp, S., and Pessin, J.E., 1997. Osmotic shock stimulates GLUT4 translocation in 3T3L1 adipocytes by a novel tyrosine kinase pathway. J. Biol. Chem. 272, 27401-27410.

7. Ciric, A., Karioti, A., Koukoulitsa, C., Sokovic, M., Skaltsa, H., 2012. Sesquiterpene Lactones from *Centaurea zuccariniana* and their antimicrobial activity. Chem. Biodiversity 9, 2843-2853.

8. Davies, S.P., Sim, A.T., Hardie, D.G., 1990. Location and function of three sites phosphorylated on rat acetyl-CoA carboxylase by the AMP-activated protein kinase. Eur. J. Biochem. 187, 183-190.

9. Di, W., Khan, M., Rasul, A., Sun, M., Sui, Y., Zhong, L., Yang, L., Zhu, Q., Feng, L., Ma, T., 2014. Isoalantolactone inhibits constitutive NF-κB activation and induces reactive oxygen species-mediated apoptosis in osteosarcoma U2OS cells through mitochondrial dysfunction. Oncol. Rep. 32, 1585-1593.

10. Dobrzyn, P., Dobrzyn, A., Miyazaki, M., Cohen, P., Asilmaz, E., Hardie, D.G., Friedman, J.M., Ntambi, J.M., 2004. Stearoyl-CoA desaturase 1 deficiency increases fatty acid

oxidation by activating AMP-activated protein kinase in liver. Proc Natl Acad Sci USA. 101, 6409-6414.

11. Engeli, S., 2012. The clinical pharmacology of obesity. Ther. Adv. Endocrinol. Metab. 3, 83-84.
12. Gowans, G.J., Hawley, S.A., Ross, F.A., Hardie, D.G., 2013. AMP is a true physiological regulator of AMP-activated protein kinase by both allosteric activation and enhancing net phosphorylation. Cell Metab. 18, 556-566.
13. Hall, M.E., Maready, M.W., Hall, J.E., Stec, D.E., 2014. Rescue of cardiac leptin receptors in db/db mice prevents myocardial triglyceride accumulation. Am. J. Physiol. Endocrinol. Metab. 307, 316-325.
14. Halseth, A.E., Ensor, N.J., White, T.A., Ross, S.A., Gulve, E.A., 2002. Acute and chronic treatment of ob/ob and db/db mice with AICAR decreases blood glucose concentrations. Biochem. Biophys. Res. Commun. 294, 798-805.
15. Hardie, D.G., 2013. AMPK: a target for drugs and natural products with effects on both diabetes and cancer. Diabetes 62, 2164-2172.
16. Hardie, D.G., Ross, F.A. Hawley, S.A., 2012. AMP-Activated Protein Kinase: A target for drugs both ancient and modern. Chemistry & Biology 19, 1222-1236.
17. Hawley, S.A., Boudeau, J., Reid, J.L., Mustard, K.J., Udd, L., Mäkelä, T.P., Alessi, D.R., Hardie, D.G., 2003. Complexes between the LKB1 tumor suppressor, STRAD aplha/beta and MO25 alpha/beta are upstream kinase in the AMP-activated protein kinase cascade. J. Biol. 2, 28.
18. Hawley, S.A., Davison, M., Woods, A., Davies, S.P., Beri, R.K., et al., 1996. Characterization of the AMP-activated protein kinase kinase from rat liver and identification

of threonine 172 as the major site at which it phosphorylates AMP activated protein kinase. J. Biol. Chem. 271, 27879-27887.

19. Himms-Hagen, J., 2004. Exercise in a pill: feasibility of energy expenditure targets. Curr. Drug Targets. CNS. Neurol. Disord. 3, 389-409.
20. Holmes, B.F., Kurth-Kraczek, E.J., Winder, W.W., 1999. Chronic activation of AMP-activated protein kinase increases GLUT-4, hexokinase, and glycogen in muscle. J. Appl. Physiol. 87, 1990-1995.
21. Horton, J.D., Goldstein, J.L., and Brown, M.S., 2002. SREBPs: activators of the complete program of cholesterol and fatty acid synthesis in the liver. J. Clin. Invest. 109, 1125-1131.
22. Huang, S., Czech, M.P., (2007). The GLUT4 glucose transporter. Cell Metab. 5, 237-252.
23. Jager, S., Handschin, C., St-Pierre, J., Spiegelman, B.M., 2007. AMP-activated protein kinase (AMPK) action in skeletal muscle via direct phosphorylation of PGC-1alpha. Proc. Natl. Acad. Sci. USA 104, 12017-12022.
24. Jiang, H.L., Chen, J., Jin, X.J., Yang, J.L., Li, Y., Yao, X.J., Wu, Q.X., 2011. Sesquiterpenoids, alantolactone analogues, and seco-guaiene from the roots of *Inula helenium*. Tetrahedron 67, 9193-9198.
25. Kahn, S.E., 2003. The relative contributions of insulin resistance and beta-cell dysfunction to the pathophysiology of Type 2 diabetes. Diabetologia 46, 3-19.
26. Kahn, S.E., Hull, R.L., Utzschneider, K.M., 2006. Mechanisms linking obesity to insulin resistance and type 2 diabetes. Nature 444, 840-846.
27. Koh, H.J., Brandauer, J., Goodyear, L.J., 2008. LKB1 and AMPK and the regulation of skeletal muscle metabolism. Curr. Opin. Clin. Nutr. Metab. Care 11, 227-232.

28. Lajter, I., Vasas, A., Beni, Z., Forgo, P., Binder, M., Bochkov, V., Zupko, I., Krupitza, G., Frisch, R., Kopp, B., et al., 2014. Sesquiterpenes from *Neurolaena lobata* and their antiproliferative and anti-inflammatory activities. J. Nat. Prod. 77, 576-582.

29. Lee, Y.S., Kim, W.S., Kim, K.H., Yoon, M.J., Cho, H.J., et al., 2006. Berberine, a natural plant product, activates AMP-activated protein kinase with beneficial metabolic effects in diabetic and insulin-resistant states. Diabetes 55: 2256-2264.

30. Li, Y., Xu, S., Mihaylova, M.M., Zheng, B., Hou, X., Jiang, B., Park, O., Luo, Z., Lefai, E., Shyy, J.Y. et al., 2011. AMPK phosphorylates and inhibits SREBP activity to attenuate hepatic steatosis and atherosclerosis in diet-induced insulin-resistant mice. Cell Metab.13, 376-388.

31. Li, Z., Qin, B., Qi, X., Mao, J., Wu, D., 2016. Isoalantolactone induces apoptosis in human breast cancer cells via ROS-mediated mitochondrial pathway and downregulation of SIRT1. Arch Pharm Res. 39, 1441-1453.

32. Ma, Y.Y., Zhao, D.G., Gao, K., 2013. Structural investigation and biological activity of sesquiterpene lactones from the traditional Chinese herb *Inula racemosa*. J. Nat. Prod. 76, 564-570.

33. Malide, D., Cushman, S.W., 1997. Morphological effects of wortmannin on the endosomal system and GLUT4-containing compartments in rat adipose cells. J. Cell. Sci. 110, 2795-2806.

34. Mosmann, T., 1983. Rapid colorimetric assay for cellular growth and survival: application to proliferation and cytotoxicity assays. J. Immunol. Methods 65: 55-63.

35. Munday, M.R., Campbell, D.G., Carling, D., and Hardie, D.G., 1998. Identification by amino acid sequencing of three major regulatory phosphorylation sites on rat acetyl-CoA carboxylase. Eur. J. Biochem. 175, 331-338.

36. Muoio, D.M., Seefeld, K., Witters, L.A., Coleman, R.A., 1999. AMP-activated kinase reciprocally regulates triacylglycerol synthesis and fatty acid oxidation in liver and muscle: evidence that sn-glycerol-3-phosphate acyltransferase is a novel target. Biochem. J. 338, 783-791.

37. Newman, D.J., Cragg, G.M., 2012. Natural products as sources of new drugs over the 30 years from 1981 to 2010. J. Nat. Prod. 75, 311-335.

38. Oakhill, J.S., Steel, R., Chen, Z.P., Scott, J.W., Ling, N., Tam, S., Kemp, B.E., 2011. AMPK is a direct adenylate charge-regulated protein kinase. Science 332, 1433-1435.

39. Pessin, J.E., Thurmond, D.C., Elmendorf, J.S., Coker, K.J., Okada, S., 1999. Molecular basis of insulin-stimulated GLUT4 vesicle trafficking. J. Biol. Chem. 274, 2593-2596.

40. Petersen, K.F. and Shulman, G.I., 2006. New insights into the pathogenesis of insulin resistance in humans using magnetic resonance spectroscopy. Obesity 14, 34S-40S.

41. Rosselli, S., Bruno, M., Raimondo, F.M., Spadaro, V., Varol, M., Koparal, A.T., Maggio, A. 2012. Cytotoxic effect of eudesmanolides isolated from flowers of *Tanacetum vulgare* ssp. siculum. Molecules 17, 8186-8195.

42. Rutter, G.A., Da Silva Xavier, G., Leclerc, I., 2003. Roles of 5'-AMP activated protein kinase (AMPK) in mammalian glucose homoeostasis. Biochem. J. 375: 1-16.

43. Seo, J.Y., Park, J., Kim, H.J., Lee, I.A., Lim, J.S., Lim, S.S., Choi, S.J., Park, J.H., Kang, H.J., Kim, J.S., 2009. Isoalantolactone from *Inula helenium* caused Nrf2-mediated induction of detoxifying enzymes. J. Med. Food. 12, 1038-1045.

44. Shaw, R.J., Kosmatka, M., Bardeesy, N., Hurley, R.L., Witters, L.A., et al., 2004. The tumor suppressor LKB1 kinase directly activates AMP-activated kinase and regulates apoptosis in response to energy stress. Proc. Natl. Acad. Sci. USA 101, 3329-3335.

45. Shaw, R.J., Lamia, K.A., Vasquez, D., Koo, S.H., Bardeesy, N., et al., 2005. The kinase LKB1 mediates glucose homeostasis in liver and therapeutic effects of metformin. Science 310: 1642-1646.

46. Shen, Y., Honma, N., Kobayashi, K., Jia, L.N., Hosono, T., Shindo, K., Ariga, T., Seki, T., 2014. Cinnamon extract enhances glucose uptake in 3T3-L1 adipocytes and C2C12 myocytes by inducing LKB1-AMP-activated protein kinase signaling. PLoS One 9, e87894.

47. Steinberg, G.R., 2007. Inflammation in obesity is the common link between defects in fatty acid metabolism and insulin resistance. Cell Cycle 6, 888-894.

48. Suwa, M., Nakano, H., Kumagai, S., 2003. Effects of chronic AICAR treatment on fiber composition, enzyme activity, UCP3, and PGC-1 in rat muscles. J. Appl. Physiol. 95, 960-968.

49. Tamrakar, A.K., Jaiswal, N., Yadav, P.P., Maurya, R., Srivastava, A.K., 2011. Pongamol from *Pongamia pinnata* stimulates glucose uptake by increasing surface GLUT4 level in skeletal muscle cells. Mol. Cell. Endocrinol. 339, 98-104.

50. Tamrakar, A.K., Schertzer, J.D., Chiu, T.T., Foley, K.P., Bilan, P.J., Philpott, D.J., Klip, A., 2010. NOD2 activation induces muscle cell-autonomous innate immune responses and insulin resistance. Endocrinology 151, 5624-5637.

51. Taniguchi, C.M., Emanuelli, B., Kahn, C.R., 2006. Critical nodes in insulin signaling pathways: insight into insulin action. Nat. Rev. Mol. Cell. Biol. 7, 85-96.

52. Terada, S., Goto, M., Kato, M., Kawanaka, K., Shimokawa, T., Tabata, I., 2002. Effects of low-intensity prolonged exercise on PGC-1 mRNA expression in rat epitrochlearis muscle. Biochem. Biophys. Res. Commun. 296, 350-354.

53. Tseng, Y.H., Cypess, A.M., Kahn, C.R., 2010. Cellular Bioenergetics as a target for obesity therapy. Nat. Rev. Drug Discov. 9, 465-482.

54. Wang, L., Hayashi, H., Kishi, K., Huang, L., Hagi, A., Tamaoka, K., Hawkins, P. T., Ebina, Y., 2000. Gi-mediated translocation of GLUT4 is independent of p85/p110α and p110 gamma phosphoinositide 3-kinases but might involve the activation of Akt kinase. Biochem. J. 345, 543-555.

55. Winder, W.W., Hardie, D.G., 1999. AMP-activated protein kinase, a metabolic master switch: possible roles in type 2 diabetes. Am. J. Physiol. 277, E1-E10.

56. Xiang, P., Guo, X., Han, Y.Y., Gao, J.M., Tang, J.J., 2016. Cytotoxic and pro-apoptotic activities of sesquiterpene lactones from *Inula britannica*. Nat. Pro. Commun. 11, 7-10.

57. Xie, Z., Dong, Y., Scholz, R., Neumann, D., Zou, M. H., 2008. Phosphorylation of LKB1 at Serine 428 by Protein Kinase C-ζ is required for Metformin-Enhanced Activation of the AMP-Activated Protein Kinase in Endothelial Cells. Circulation 117, 952-962.

58. Yeh, J.I., Gulve, E.A., Rameh, L., Birnbaum, M.J., 1995. The effects of wortmannin on rat skeletal muscle. Dissociation of signaling pathways for insulin- and contraction-activated hexose transport. J. Biol. Chem. 270, 2107-2111.

59. Yu, C., Chen, Y., Cline, G.W., Zhang, D., Zong, H., Wang, Y., Bergeron, R., Kim, J.K., Cushman, S.W., Cooney, G.J. et al., 2002. Mechanism by which fatty acids inhibit insulin activation of insulin receptor substrate-1 (IRS-1)-associated phosphatidylinositol 3-kinase activity in muscle. J. Biol. Chem. 277, 50230-50236.

60. Zong, H., Ren, J.M., Young, L.H., Pypaert, M., Mu, J., Birnbaum, M.J., Shulman, G.I., 2002. AMP kinase is required for mitochondrial biogenesis in skeletal muscle in response to chronic energy deprivation. Proc. Natl. Acad. Sci. USA 99, 15983-15987.

**Figure legends**

**Figure 1: (A)** Chemical structure of isoalantolactone (K007), isolated from the roots of *Inula racemosa*. **(B)** Effect of K007 on 2-deoxyglucose uptake in L6 myotubes. Cells were incubated for 16h with increasing concentrations of K007. After incubation cells were left untreated (white bars) or stimulated with insulin (100 nM) for 20 min (Black bars), followed by the determination of 2-DG uptake. Results are expressed as fold stimulation over control basal. Results shown are mean ± SEM of three independent experiments. *P<0.05, **P<0.01 relative to respective control condition. **(C)** Effect of K007 on cell viability of L6 myotubes. Cells were treated for 16h with indicated concentrations of K007, followed by determination of cell viability by MTT assay. Results shown are mean ± SEM (n=3). ***P<0.001 relative to control. **Scheme 1** for the synthesis of derivatives of K007 (**2a-2h**) via Michael addition.

**Figure 2:** Scheme 2 for the **s**ynthesis of alloalantolactone (**5**) and Scheme 3 for the **s**ynthesis of ester analogues of K007 (**4a-4d**) via allylic hydroxylation.

**Figure 3: (A** &**B)** Effect of **4a** on glucose uptake in L6 myotubes. Cells were incubated with **4a** for 16h **(A)** or various time duration **(B)** at increasing concentrations **(A)** or at 5μM concentration **(B)**. After incubation cells were left untreated (white bars) or stimulated with insulin (100 nM) for 20 min (Black bars), followed by the determination of 2-DG uptake. Results are expressed as fold stimulation over control basal. Results shown are mean ± SEM (n=3) *P<0.05, ***P<0.001 relative to respective control condition. **(C)** Effect of **4a** on cell viability of L6 myotubes. Cells were treated for 16h with indicated concentrations of **4a**, followed by determination of cell viability by MTT assay. Results shown are mean ± SEM (n=3). **(D)** Effect of **4a** on GLUT4

translocation to cell surface in L6-GLUT4*myc* myotubes. Cells were incubated with **4a** at indicated concentrations for 16h. After incubation cells were left untreated (white bars) or stimulated with insulin (100 nM) for 20 min (Black bars), followed by the determination of the surface level of GLUT4*myc*. Results are expressed as fold stimulation over control basal. Results shown are mean ± SEM (n=3). **P<0.01, ***P<0.001 relative to respective control condition. **(E&F)** Effect of **4a** on total amount of GLUT4 **(E)** and GLUT1 **(F)** in L6 myotubes. Cells were incubated with **4a** at indicated concentrations for 16h. After incubation cells were left untreated (white bars) or stimulated with insulin (100 nM) for 20 min (Black bars), followed by cell lysis and Western analysis. Shown are representative immunoblots and densitometric quantification of GLUT4 and GLUT1 relative to actinin-1. Results of three independent experiments are presented as mean ± SEM.

**Figure 4: (A)** Effect of **4a** on PI-3-K mediated signaling pathway. L6 myotubes were treated with **4a** (overnight) or insulin (20 min) in absence (white bars) or presence (black bars) of wortmannin and the rate of glucose uptake was determined. Results are expressed as fold stimulation over control without wortmannin. Results shown are mean ± SEM (n=3). **P<0.01 relative to control without wortmannin, $^{\#\#}$P<0.01 relative to insulin treatment without wortmannin. **(B-D)** Effect of **4a** on Akt phosphorylation. L6 myotubes were treated with **4a** (overnight) or insulin (20 min) in absence (-W, white bars) or presence (+W, black bars) of wortmannin, followed by cell lysis and Western analysis. Shown are representative immunoblots and densitometric quantification of phospho-Akt (Ser-473) and phospho-Akt (Thr-308) relative to total Akt. Results of three independent experiments are presented as mean ± SEM.

**Figure 5:** Effect of **4a** on AMPK mediated signaling pathway. **(A)** L6 myotubes were treated overnight with **4a** or metformin in absence (white bars) or presence (black bars) of dorsomorphin and the rate of glucose uptake was determined. Results are expressed as fold stimulation over control without dorsomorphin. Results shown are mean ± SEM (n=3). **P<0.01 relative to control without dorsomorphin, $^{\#\#}$P<0.01relative to respective without dorsomorphin condition. **(B, C, E, F)** Effect of **4a** on phosphorylation of AMPK (Thr-172) and its upstream (LKB1, Ser-428) and downstream (ACC, Ser-79; SREBP-1c, Ser-372) targets. Cells were incubated with **4a** at indicated concentrations for 16h, followed by cell lysis and Western analysis. Shown are representative immunoblots and densitometric quantification of phospho-AMPK relative to total AMPK **(B)**, phospho-LKB-1 relative to Actinin-1 **(C)**, phospho-ACC relative to total ACC **(E)** and phospho-SREBP-1c relative to Actinin-1 **(F)**. Results of three independent experiments are presented as mean ± SEM. *P<0.05, **P<0.01 relative to control. **(D)** Effect of **4a** on cellular ATP level in L6 myotubes. Cells were treated with **4a** at indicated concentrations for 16h, followed by cell lysis and determination of cellular ATP level. Results shown are mean ± SEM (n=3). *P<0.05 relative to control.

**Figure 6:** Metabolic effects of **4a** administration in db/db mice. **(A** & **B)** Effect on body weight and random blood glucose level every three days during course of treatment (n=5). **(C)** Oral glucose tolerance test on db/db mice after 15 days treatment with **4a** after overnight fast (n=5). **(D)** The bar graph represents the average area under curve (n=5). **(E & F)** Effect of **4a** on expression of genes related to glucose uptake in skeletal muscle. Representative images of RT-PCR products **(E)** and densitometric quantification of transcript of GLUT4 and hexokinase **(F)** are shown. Data are mean ± SEM relative to 18S RNA of three mice. **(G)** Effect of **4a** on body

mass. After 15 days treatment with **4a**, animals were subjected to whole body composition analysis by Echo-MRI. Data are mean ± SEM (n=5). **(H & I)** Effect of 4a on total amount of GLUT4 and hexokinase II in skeletal muscle of db/db mice. After 15 days treatment with **4a**, the skeletal muscle tissue sample was dissected out and subjected to Western analysis. Shown are representative immunoblots and densitometric quantification of GLUT4 **(H)** and hexokinase II **(I)** relative to β-Actin. *P<0.05 relative to control animals. **(J)** Serum insulin concentration of mice after treatment with **4a**. Data are mean ± SEM (n=4).

**Figure 7: (A-G)** Effect of **4a** treatment on AMPK signaling in skeletal muscle **(A-D)** and liver **(E-G)** of db/db mice. After 15 days treatment with **4a**, the skeletal muscle and liver tissue samples were dissected out and subjected to Western analysis. Shown are representative immunoblots **(A & E)** and densitometric quantification of phospho-AMPK relative to total AMPK **(B & F)**, phospho-ACC relative to total ACC **(C & G)**, and phospho-LKB-1 relative to β-Actin **(D)**. *P<0.05, **P<0.01 relative to control animals. **(H-L)** Effect of **4a** treatment on cholesterol and triglyceride content in serum and tissue samples of db/db mice. Data are presented as mean ± SEM (n=4). *P<0.05, **P<0.01, ***P<0.001 relative to control animals.

**Figure 8:** Effect of **4a** treatment on expression of genes related to lipid metabolism in liver samples of db/db mice. Representative images of RT-PCR products and densitometric quantification of the transcripts are presented. Data are mean ± SEM relative to 18S RNA of three mice.

**Figure 9:** Effect of **4a** on energy expenditure in db/db mice. After 15 days treatment with **4a** (30 mg/kg body weight), energy expenditure was evaluated by measuring the carbon dioxide release **(A)**, oxygen consumption **(C)**, respiration exchange ratio **(E)** over a 24h period. Energy expenditure expressed as kCal/ 30 min/animal **(G)** was calculated using equation described in method section. The adjacent bar graphs **(B, D, F** and **H)** represent the average for each group (n=5). *P<0.05, **P<0.01 relative to respective control animals.

**Figure 10:** Effect of **4a** on energy expenditure in db/db mice (contd). Physical activity of the animals was expressed as x axis and z axis movement measured by breaking of successive beams over 3-days period **(A** & **B)**. Resting $VO_2$ measured during none to less than baseline activity (0–10 counts/10 min) served as a measure of basal or resting metabolic rate **(C** & **D)**. Food consumption was expressed as gram/ cycle through a 12h light/dark cycle **(E)**, over 3-days period (n=5). **P<0.01, ***P<0.001 relative to control animals.

**Figure 11: (A-D)** Effect of **4a** treatment on gene expression of the transcription factors and mitochondrial markers in skeletal muscle of db/db mice. Representative images of RT-PCR products **(A** & **C)** and densitometric quantification of the transcripts **(B** &**D)** are presented. Data are mean ± SEM relative to 18S RNA of three mice. **(E-G)** Representative immunoblots and densitometric quantification of mitochondrial markers relative to β-actin are shown. *P<0.05, ***P<0.001 relative to control animals.

**Figure 12:** Schematic representation of the biological effects of **4a** on clonal skeletal muscle cells and db/db mice.

**Table 1:** Sequences of primers used for semi quantitative RT- PCR

| Gene | Primer Forward | Primer Reverse |
|---|---|---|
| PGC-1α | TCAGAACCATGCAGCAAACC | TTGGTGTGAGGAGGGTCATC |
| UCP1 | ATGACGTCCCCTGCCATTTA | GGTGTACATGGACATCGCAC |
| COX IV | GGTTTATTCAGGGAGGGGCT | CTCCCAAATCAGAACGAGCG |
| NRF1 | AAATCGTTCCTCAGCCTCCA | CACACACCCTGCACTTACAC |
| DIO2 | TGGAGAAAGGACAGGCAGAG | GCTGTAAGGGTAGGGGTTGT |
| PPAR α | AGCTTGTGGTCGTGTGTCTA | GCTTAGGGACAGTGACAGGT |
| Cytochrome C | CCTGCCTGGTGTTAAGAGGA | CACTGGGCACACTTCTGAAC |
| ATP Synthase | CCGGGCAAGAAAGATACAGC | GTCCCACCATGTAGAAGGCT |
| Hexokinase | AGTGGAAGCCAGCTTTTTGA | TTCAGCAGCTTGACCACATC |
| GLUT 4 | ACTCTTGCCACACAGGCTCT | AATGGAGACTGATGCGCTCT |
| 18S RNA | CGCGGTTCTATTTTGTTGGT | AGTCGGCATCGTTTATGGTC |
| Scd1 | CTTCAAGGGCAGTTCTGAGG | CAATGGTTTTCATGGCAGTG |
| ACC1 | GCCTCTTCCTGACAAACGAG | TGACTGCCGAAACATCTCTG |
| Srebp1c | GATCAAAGAGGAGCCAGTGC | TAGATGGTGGCTGCTGAGTG |
| PPARα | AGCTTGTGGTCGTGTGTCTA | GCTTAGGGACAGTGACAGGT |

**Table 2:** Effect of isoalantolactone (**1**) and its derivatives on glucose uptake in L6 myotubes.

| **Compound No.** | **Compound structure** | **Concentration** | **Glucose uptake stimulation (fold over control)** |
|---|---|---|---|
| 1 | 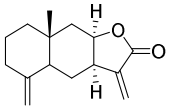 | 5µM | **2.10** |
| 2a | 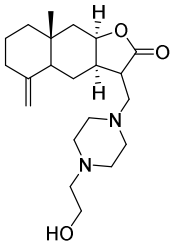 | 5µM | 1.31 |
| 2b | 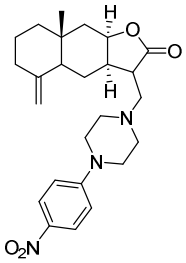 | 5µM | 1.33 |
| 2c | 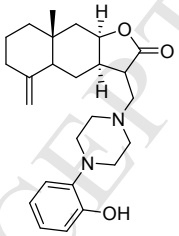 | 5µM | 1.26 |
| 2d | 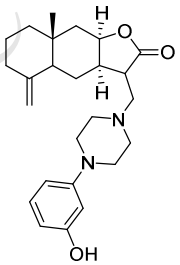 | 5µM | 1.17 |

| | | | |
|---|---|---|---|
| 2e | 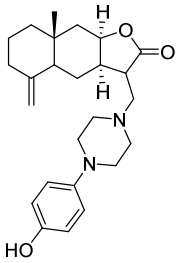 | 5μM | 0.98 |
| 2f | 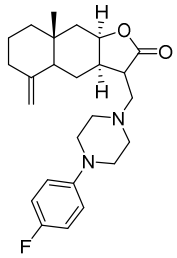 | 5μM | 1.37 |
| 2g | 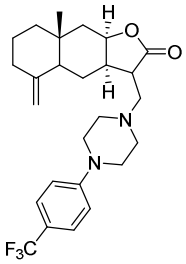 | 5μM | 1.15 |
| 2h | 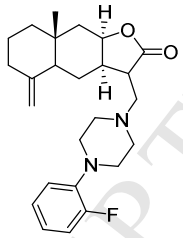 | 5μM | 1.27 |
| 3 | 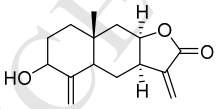 | 5μM | **1.60** |
| 4a | 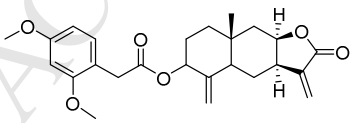 | 5μM | **3.55** |
| 4b | 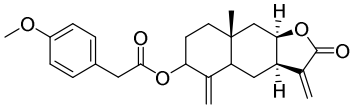 | 5μM | **2.20** |

| | | | |
|---|---|---|---|
| 4c | 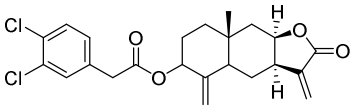 | 5μM | **2.54** |
| 4d | 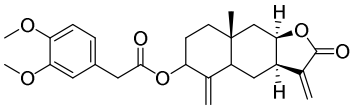 | 5μM | 1.48 |
| 5 | 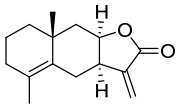 | 5μM | 1.54 |

**Figure # 11**

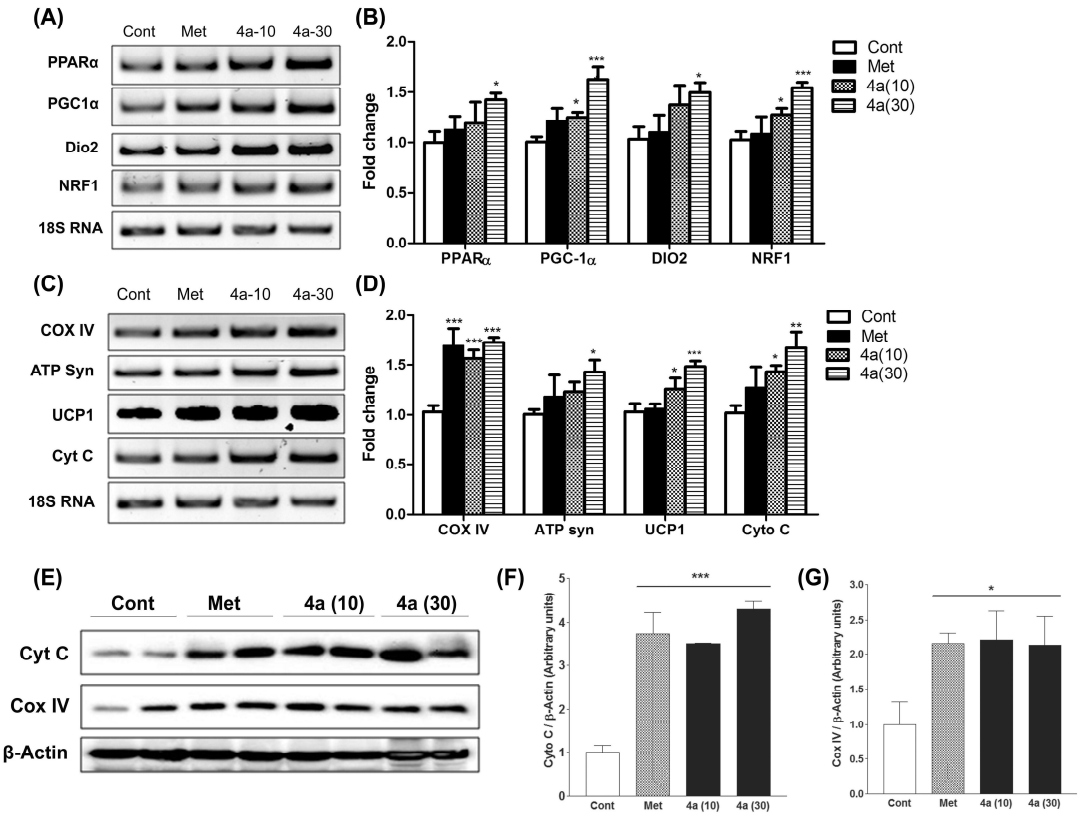

**Figure # 1**

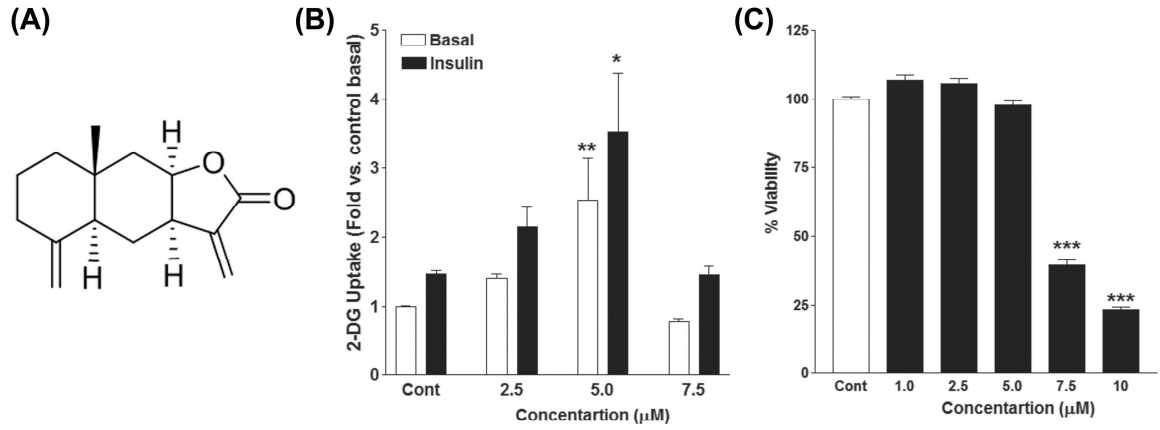


**Scheme: 1**

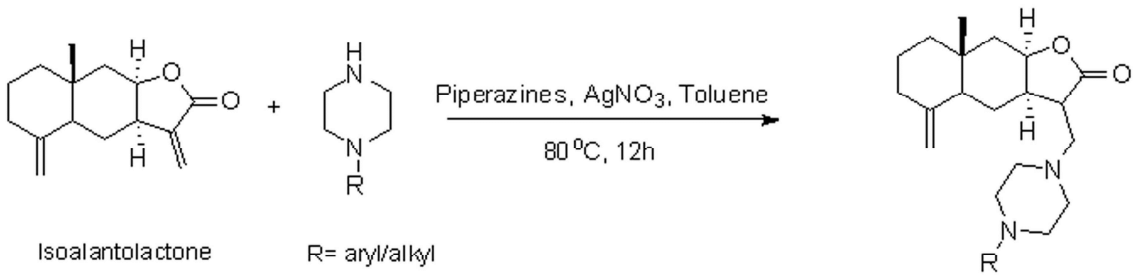


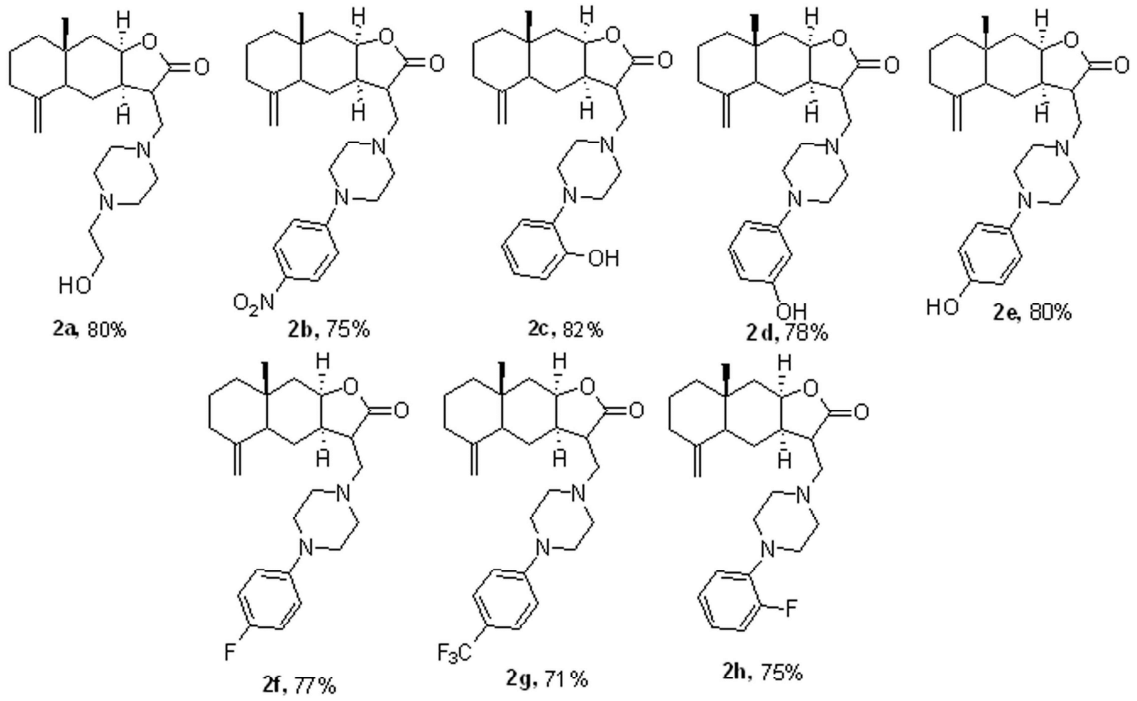

## Figure # 10

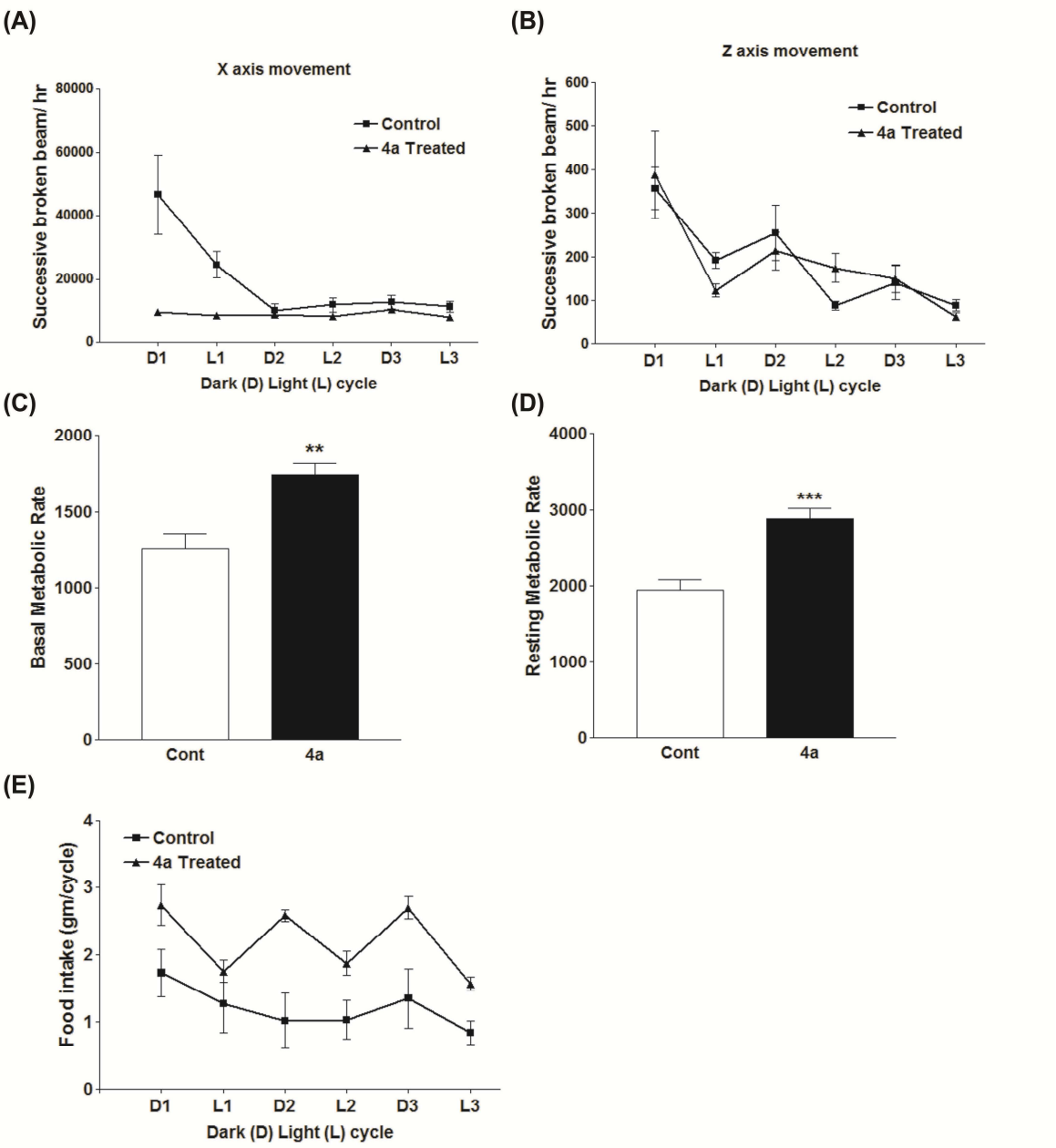
(A)
X axis movement
Successive broken beam/ hr
80000
60000
40000
20000
0
Control
4a Treated
D1
L1
D2
L2
D3
L3
Dark (D) Light (L) cycle
(B)
Z axis movement
Successive broken beam/ hr
600
500
400
300
200
100
0
Control
4a Treated
D1
L1
D2
L2
D3
L3
Dark (D) Light (L) cycle
(C)
Basal Metabolic Rate
2000
1500
1000
500
0
**
Cont
4a
(D)
Resting Metabolic Rate
4000
3000
2000
1000
0
***
Cont
4a
(E)
Food intake (gm/cycle)
4
3
2
1
0
Control
4a Treated
D1
L1
D2
L2
D3
L3
Dark (D) Light (L) cycle

**Figure # 12**

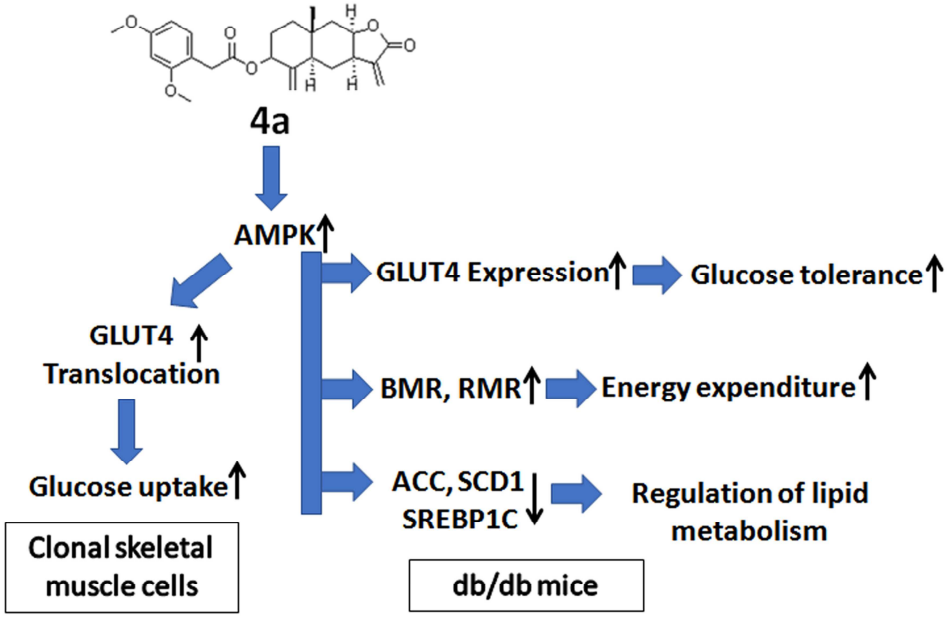

**Figure # 2**

**Scheme: 2**

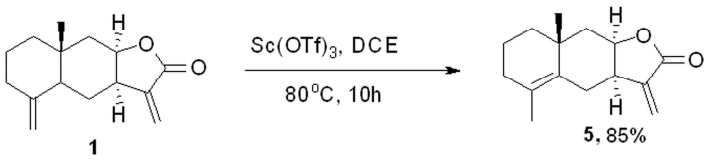


**Scheme :3**

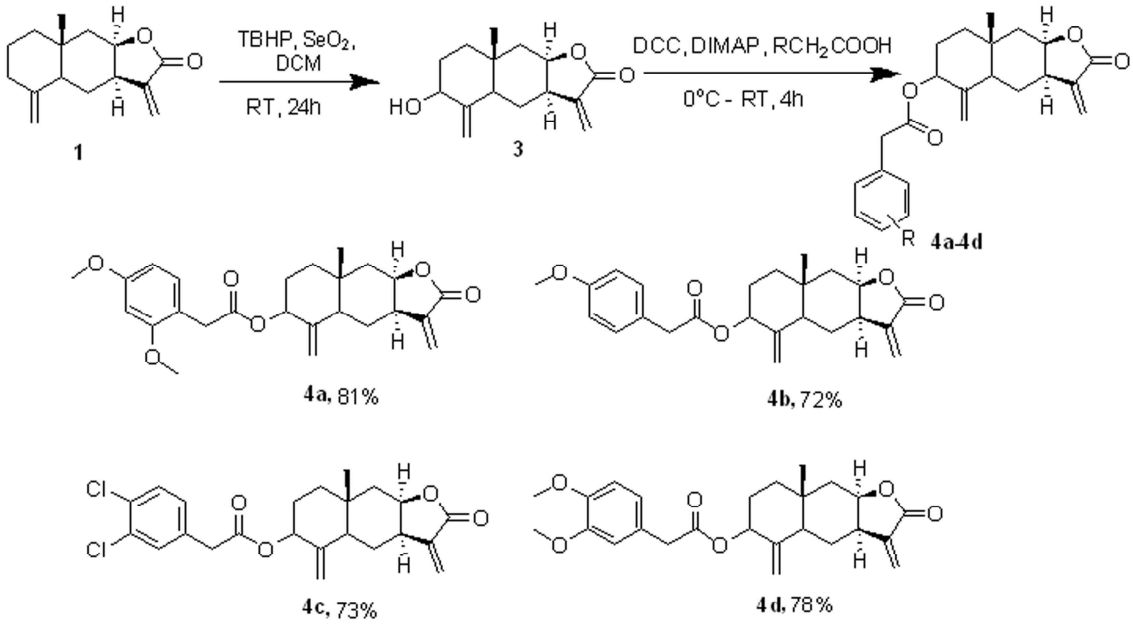

**Figure # 3**

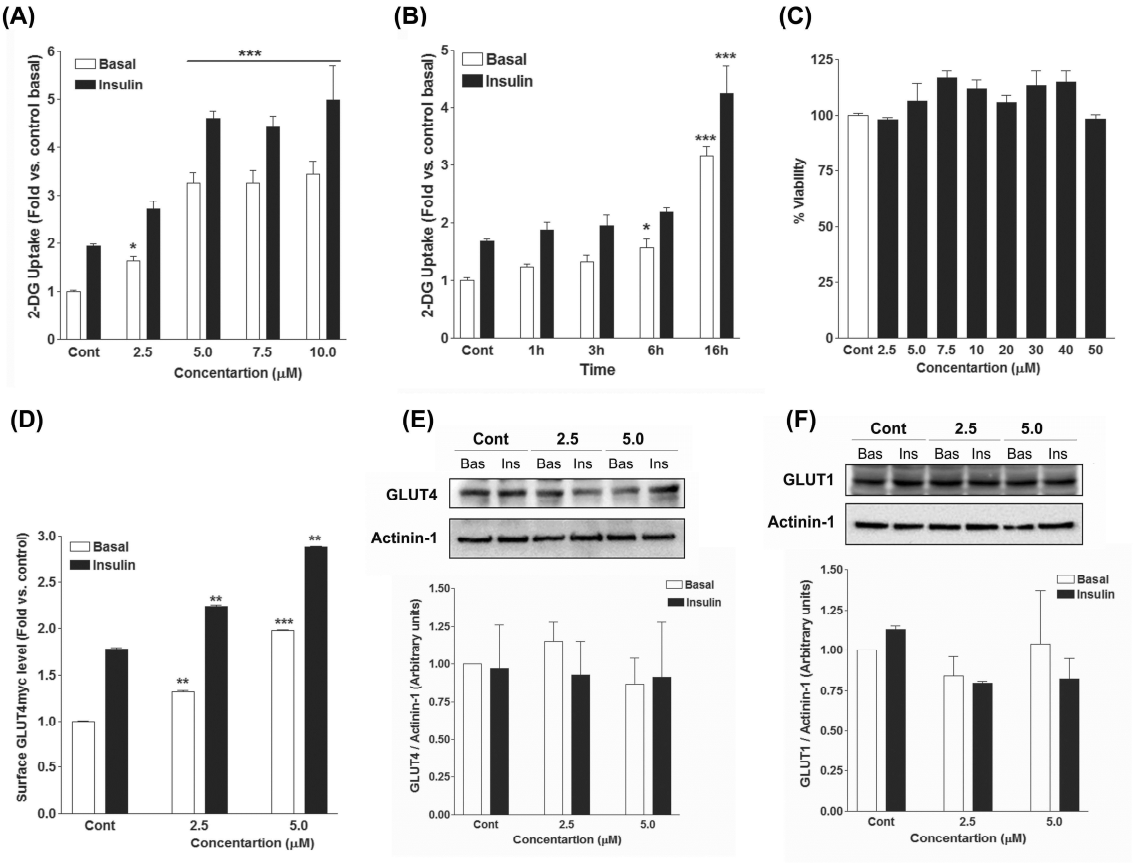

## Figure # 4

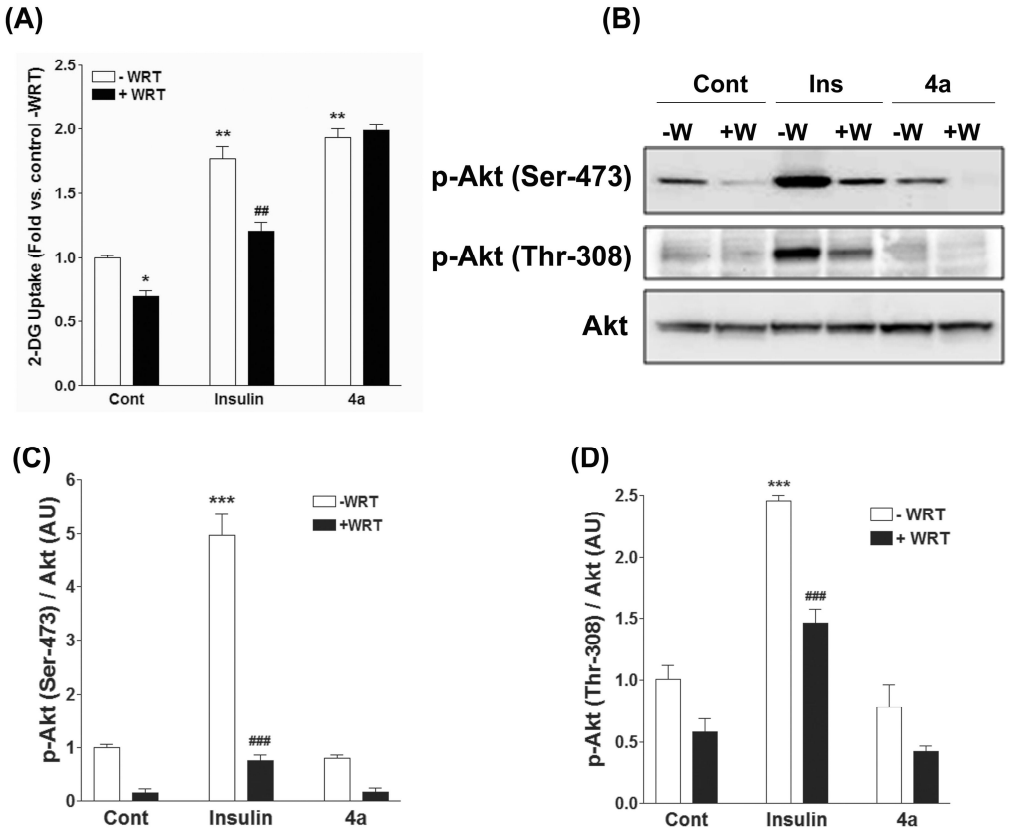

**Figure # 5**

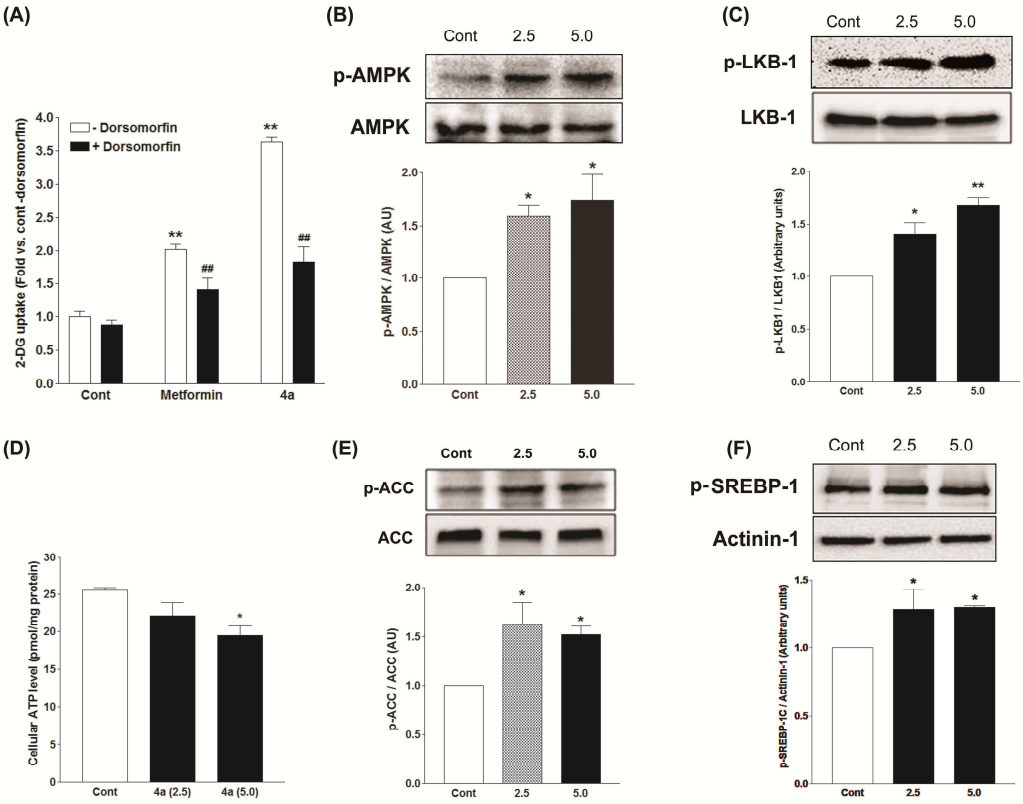

**Figure # 6**

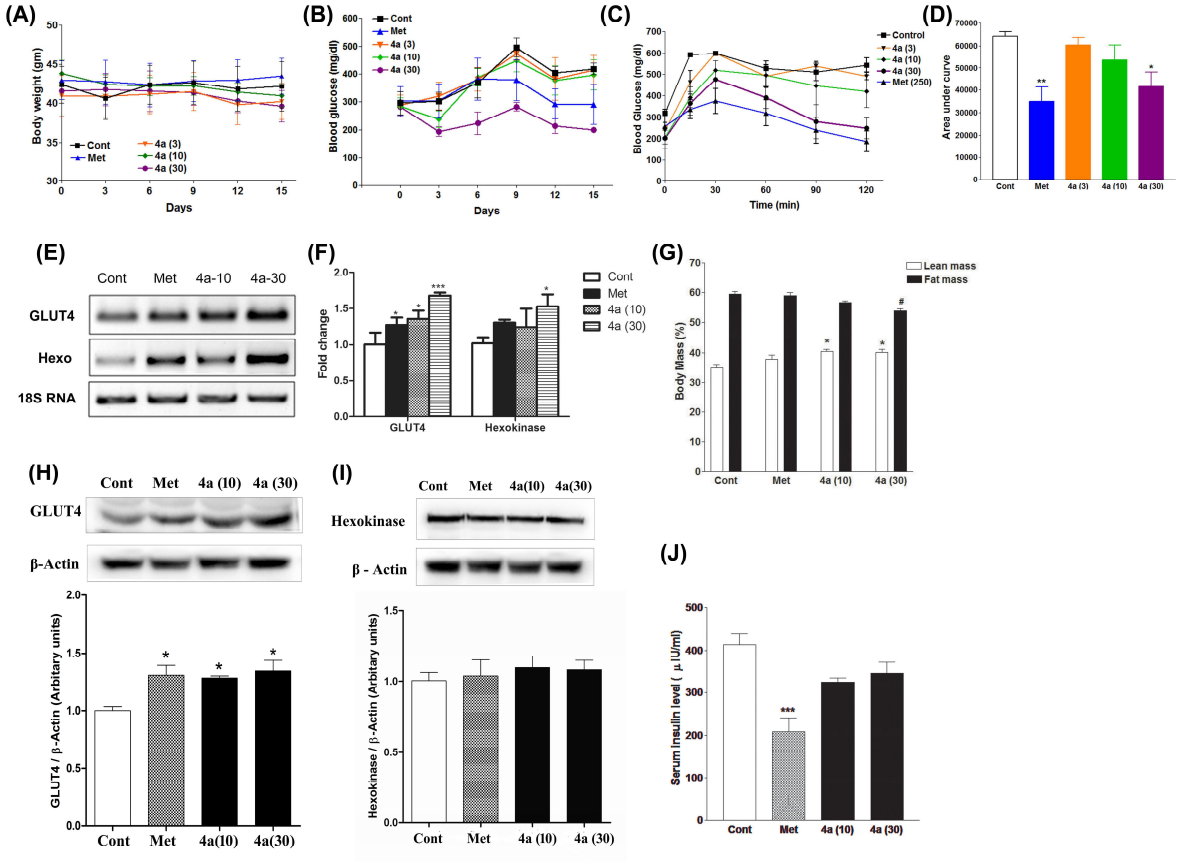

**Figure # 7**

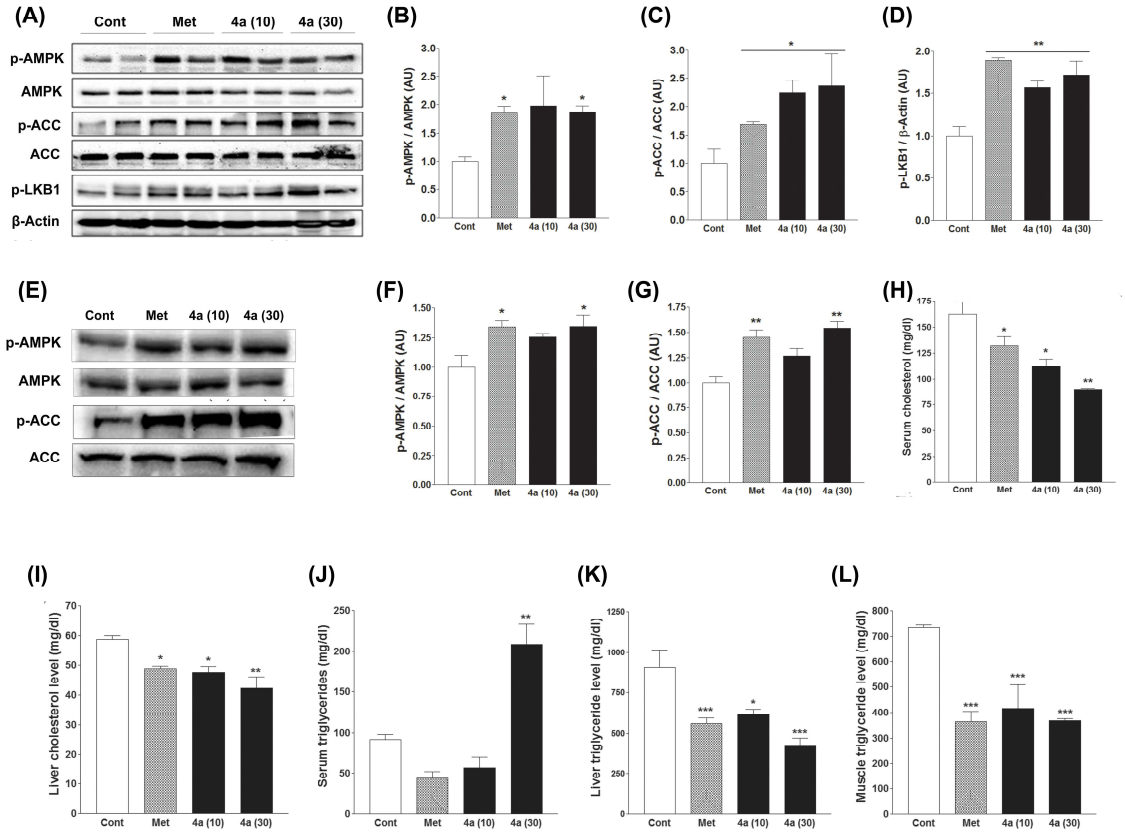

**Figure # 8**

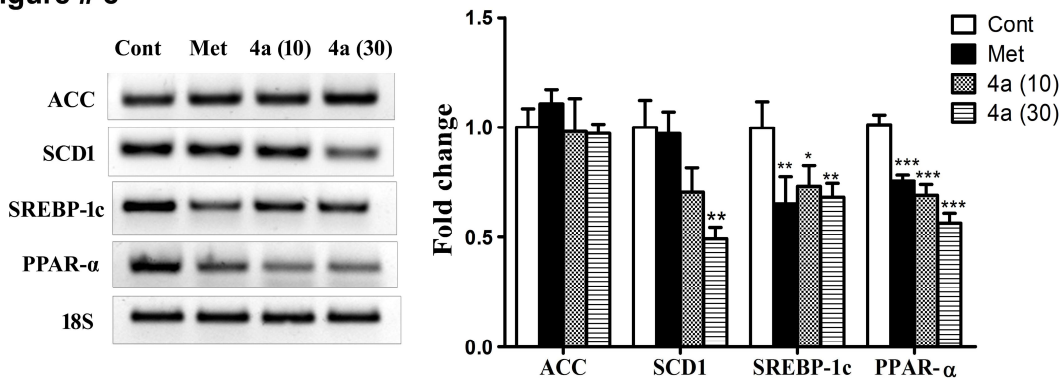

## Figure # 9

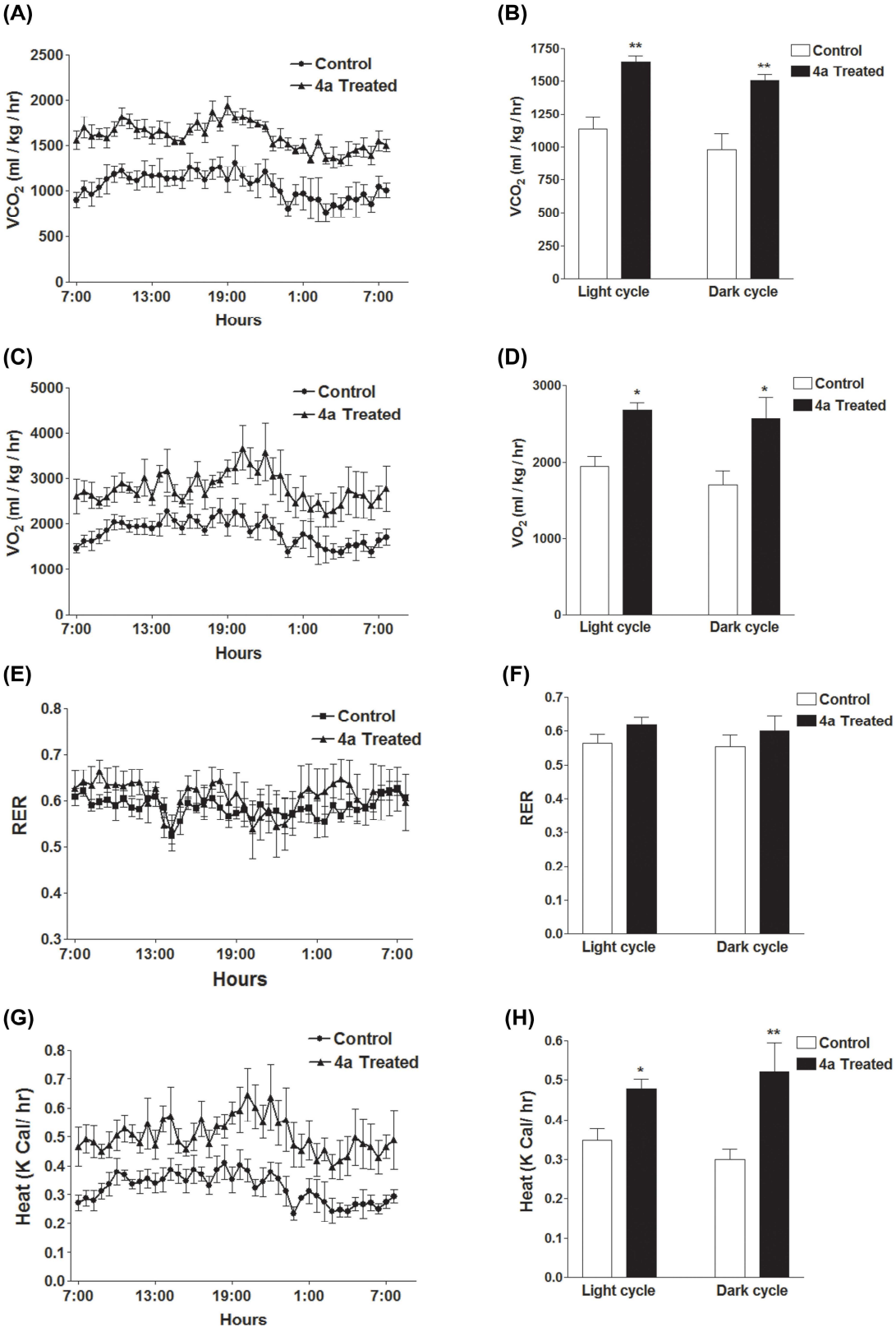
(A)
Control
4a Treated
VCO2 (ml / kg / hr)
2500
2000
1500
1000
500
0
7:00
13:00
19:00
1:00
7:00
Hours
(B)
Control
4a Treated
VCO2 (ml / kg / hr)
1750
1500
1250
1000
750
500
250
0
**
**
Light cycle
Dark cycle
(C)
Control
4a Treated
VO2 (ml / kg / hr)
5000
4000
3000
2000
1000
0
7:00
13:00
19:00
1:00
7:00
Hours
(D)
Control
4a Treated
VO2 (ml / kg / hr)
3000
2000
1000
0
*
*
Light cycle
Dark cycle
(E)
Control
4a Treated
RER
0.8
0.7
0.6
0.5
0.4
0.3
7:00
13:00
19:00
1:00
7:00
Hours
(F)
Control
4a Treated
RER
0.7
0.6
0.5
0.4
0.3
0.2
0.1
0.0
Light cycle
Dark cycle
(G)
Control
4a Treated
Heat (K Cal/ hr)
0.8
0.7
0.6
0.5
0.4
0.3
0.2
0.1
0.0
7:00
13:00
19:00
1:00
7:00
Hours
(H)
Control
4a Treated
Heat (K Cal/ hr)
0.6
0.5
0.4
0.3
0.2
0.1
0.0
*
**
Light cycle
Dark cycle

**Highlights**

- Chemical derivative of isoalantolactone (**4a**) stimulates glucose utilization in skeletal muscle.
- The mechanism relies on enhanced translocation of GLUT4 to cell surface driven by LKB1/AMPK-dependent signaling.
- **4a** improves blood glucose level, body mass index, lipid parameters and glucose tolerance in db/db mice.
- **4a** increases energy expenditure via activating substrate utilization in db/db mice.